Complexity of spatiotemporal traffic phenomena in flow of identical drivers: Explanation based on fundamental hypothesis of three-phase theory

Boris S. Kerner
Daimler AG, GR/PTF, HPC: G021, 71059 Sindelfingen, Germany
(Received 11 January 2012; published 23 March 2012)

Based on numerical simulations of a stochastic three-phase traffic flow model, we reveal the physics of the fundamental hypothesis of three-phase theory that, in contrast with a fundamental diagram of classical traffic flow theories, postulates the existence of a two-dimensional (2D) region of steady states of synchronized flow where a driver makes an arbitrary choice of a space gap (time headway) to the preceding vehicle. We find that macroscopic and microscopic spatiotemporal effects of the *entire complexity* of traffic congestion observed up to now in real measured traffic data can be explained by simulations of traffic flow consisting of *identical* drivers and vehicles, if a microscopic model used in these simulations incorporates the fundamental hypothesis of three-phase theory. It is shown that the driver's choice of space gaps within the 2D region of synchronized flow associated with the fundamental hypothesis of three-phase theory can qualitatively change types of congested patterns that can emerge at a highway bottleneck. In particular, if drivers choose long enough spaces gaps associated with the fundamental hypothesis, then general patterns, which consist of synchronized flow and wide moving jams, do not emerge independent of the flow rates and bottleneck characteristics: Even at a heavy bottleneck leading to a very low speed within congested patterns, only synchronized flow patterns occur in which no wide moving jams emerge spontaneously.

DOI: 10.1103/PhysRevE.85.036110 PACS number(s): 89.40.−a, 47.54.−r, 64.60.Cn, 05.65.+b

I. INTRODUCTION: FUNDAMENTAL HYPOTHESIS OF THREE-PHASE THEORY

In hypothetical car following with nondisturbed and noiseless vehicle motion with a constant speed, classical traffic flow theories and models (see books and reviews in Ref. [1]) assume the existence of a space-gap–speed relationship associated with a fundamental diagram for traffic flow. The space-gap–speed relationship determines a single (called sometimes optimal or safe) space gap (time headway) for each given speed [1]: When the gap is greater than the optimal one, the vehicle accelerates; when the gap is smaller than the optimal one, the vehicle decelerates. The space-gap–speed relationship is a driver model characteristic [2].

In empirical observations, spontaneous traffic breakdown at a highway bottleneck leading to congested traffic is a local phase transition from free flow (F) to synchronized flow (S) (F → S transition) [3–6]. Rather than an F → S transition, in traffic flow models with a fundamental diagram explaining traffic breakdown through free-flow instability [1] traffic breakdown is a local phase transition from free flow to a wide moving jam (J) (F → J transition) (see Sec. 10.3 of Ref. [6]); these models are often called *two-phase* traffic flow models.

Because the two-phase models cannot explain traffic breakdown as observed in real measured traffic data, the author introduced three-phase traffic theory [3,5] in which there are (1) the free flow, (2) synchronized flow, and (3) wide moving jam phases. The synchronized flow and wide moving jam phases associated with congested traffic are defined via the empirical definitions [S] and [J], respectively. A wide moving jam is a moving traffic jam, i.e., a localized structure of great vehicle density and low speed, spatially limited by two jam fronts, which exhibits the characteristic jam feature [J] to propagate through bottlenecks while maintaining the mean velocity of the downstream jam front. Synchronized flow [S] is defined as congested traffic that does not exhibit the jam feature [J]; in particular, the downstream front of synchronized flow is often *fixed* at the bottleneck. First, three-phase microscopic traffic flow models were introduced in Refs. [7,8]. Over time there have been developed a number of three-phase traffic models (e.g., Refs. [9–49]).

In contrast with two-phase models with a fundamental diagram that assume the existence of a space-gap–speed relationship [1], the fundamental hypothesis of three-phase traffic theory [3–6] assumes the existence of a two-dimensional (2D) region of hypothetical homogeneous synchronized flow [50] in the space-gap–speed plane restricted by a synchronization space gap G and safe gap g_{safe}, where $G > g_{\text{safe}}$ at any synchronized flow speed [Fig. 1(a)]. When the space gap g between the vehicle and the preceding vehicle $g > G$, the vehicle accelerates ["acceleration" in Fig. 1(a)]. When $g < g_{\text{safe}}$, the vehicle decelerates ("deceleration"). When a driver approaches a slower-moving preceding vehicle and he or she cannot overtake it, then the driver begins to decelerate, adapting its speed to the speed of the preceding vehicle, when the gap g to the preceding vehicle becomes smaller than the synchronization gap G. This driver's speed adaptation occurs under condition ("speed adaptation" in Fig. 1)

$$g_{\text{safe}} \leqslant g \leqslant G. \tag{1}$$

Therefore, the fundamental hypothesis of three-phase theory states that a driver makes an *arbitrary choice* in the space gap (time headway) within the gap range (1) [3–6].

In numerical simulations with three-phase models, a synchronized flow pattern (SP) that consists of the synchronized flow phase only [Fig. 2(a)] transforms into a general pattern (GP) that consists of both synchronized flow and wide moving jam phases [Fig. 2(b)]. This occurs when the bottleneck strength that characterizes the effect of the bottleneck on traffic flow increases, and, respectively, the speed decreases

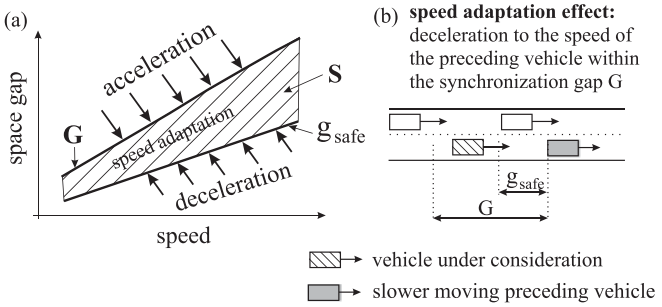

FIG. 1. Fundamental hypothesis and associated driver's speed adaptation effect within 2D region of homogeneous synchronized flow [5,6]: Qualitative explanation of synchronization G and safe gaps g_{safe} in the space-gap–speed plane (a) and of driver's speed adaptation under condition (1) (b).

and density increases within the SP [Fig. 2(c)] [51]. However, in some traffic observations of synchronized flow no wide moving jams emerge independent of the speed and density of the synchronized flow [5]. In addition, there can be a complex transformation between SPs and GPs over time at an almost time-independent bottleneck strength and the flow rate in free flow upstream of a bottleneck q_{in} (see Chap. 13 of Ref. [5]). This complexity of spatiotemporal traffic congestion found in measured traffic data has not been explained up to now.

It must be noted that three-phase traffic flow models in the framework of the fundamental diagram approach (when an infinite number of 2D steady states of synchronized flow are

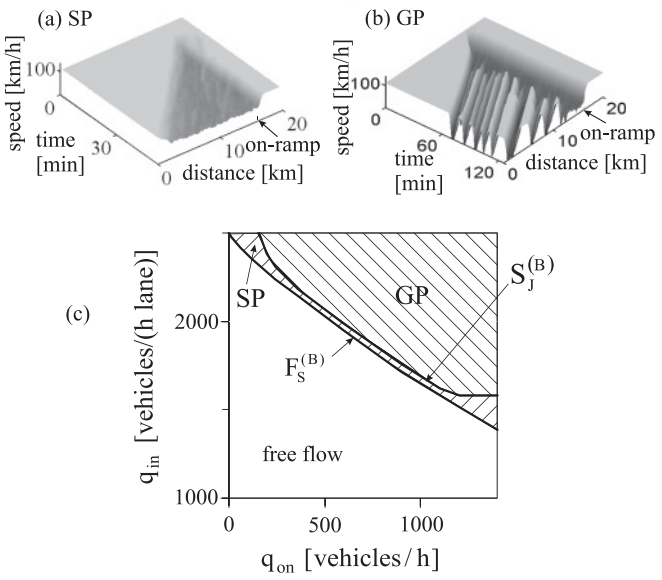

FIG. 2. Simulations of the transformation of an SP (a) into an GP (b) at on-ramp bottleneck with a three-phase model under an increase in on-ramp inflow q_{on} (increase in bottleneck strength) [5,6]. (c) Simplified diagram of congested patterns in the flow-flow plane: At the boundary $F_S^{(B)}$ of this diagram an SP occurs spontaneously (a); when q_{on} increases, then at the diagram boundary $S_J^{(B)}$ wide moving jams emerge spontaneously within synchronized flow of the SP, i.e., the SP transforms into an GP (b). In (a), (b) speeds in space and time in the left road lane are shown. q_{in} is the flow rate (per lane) in free flow on main road upstream of the congested pattern.

averaged to one synchronized flow speed for each density) can also be developed that can show an F → S transition as well as the transformation of an SP into an GP similar to that shown in Fig. 2 [13,52]. Thus a question arises [53]: What is the physical sense of the fundamental hypothesis of three-phase theory? This critical question about three-phase theory addressed in the literature as well as the above-mentioned complexity of pattern transformation observed in measured data that has not been fully explained hinder the further understanding of the physics of vehicular traffic.

In this article we will try to show that the *entire complexity* of empirical spatiotemporal traffic congestion observed up to now in real highway traffic [4,5,54,55] can be simulated with a three-phase model of traffic flow consisting of *identical* drivers and vehicles [56], *if the model incorporates the fundamental hypothesis of three-phase theory*. This will also explain the physics behind the fundamental hypothesis of three-phase theory.

The article is organized as follows. In Sec. II we show that under application of the fundamental hypothesis of three-phase theory, simulations of traffic flow of identical drivers made at the same given flow rates, the same bottlenecks and other traffic parameters can explain the complexity of spatiotemporal traffic congestion observed in real measured data. The physics of the effect of the fundamental hypothesis on simulations of these traffic phenomena is the subject of Sec. III. In discussion, Sec. IV, we consider random jam emergence in synchronized flow associated with the fundamental hypothesis as well as explain why the fundamental hypothesis is the result of the empirical phase definitions [S] and [J].

II. COMPLEXITY OF SPATIOTEMPORAL TRAFFIC CONGESTION

Complex spatiotemporal transformations between GPs and SPs are usual traffic phenomena observed in macroscopic traffic data measured by road detectors [5]. In many cases, there are no considerable changes in flow rates and other traffic macroscopic parameters that could explain these diverse complex transformations between qualitatively different congested traffic patterns (see chaps. 13 and 14 of [5]). As we will see below, complex microscopic spatiotemporal jam dynamics in synchronized flow, in particular, the interruption of jam growth and random moving jam dissolution in synchronized flow, are also observed in empirical single-vehicle data. We show in this section that macroscopic and microscopic spatiotemporal effects of the *entire complexity* of traffic congestion observed up to now in real measured traffic data can be explained by simulations of traffic flow consisting of *identical* drivers and vehicles, if a microscopic model used in these simulations incorporates the fundamental hypothesis of three-phase theory. This is a physical effect of the application of the fundamental hypothesis of three-phase theory on simulated spatiotemporal traffic phenomena [53].

In the article all simulations have been made with a discrete version of the Kerner-Klenov stochastic microscopic three-phase model [7,57–59]. Because this model has been discussed in detail in Refs. [58,59], we have presented the model and model parameters in Appendix A.

To simulate the driver's choice of a space gap within the 2D region of synchronized flow [Fig. 1(a)], we use a stochastic description of driver's speed adaptation within this 2D region made in the Kerner-Klenov model [7,57–59]. The physical meaning of the stochastic description of the driver's speed adaptation within the synchronization gap, explained in more detail in Appendix B, is as follows: The driver behavior to adapt its speed to the speed of the preceding vehicle moving within the 2D region of synchronized flow is described by probability p_2 for continuous deceleration to the speed of the preceding vehicle as well as by probability p_1 for the beginning of this deceleration. The greater the probabilities p_2 and/or p_1, the stronger on average the adaptation of the vehicle speed to the speed of the preceding vehicle and, therefore, the larger on average the space gap within the 2D region of synchronized flow that the driver chooses.

A. Random spatiotemporal transformations between diverse congested patterns in empirical single-vehicle data and microscopic simulations

Random spatiotemporal transformations between diverse congested patterns is the phenomenon that is often observed in real empirical congested patterns measured on highways with many adjacent bottlenecks (see examples of empirical macroscopic data in chap. 19 of Ref. [5]). Such pattern transformations can also be found in empirical NGSIM data [54] as shown in Fig. 3.

As mentioned in Ref. [58], the significance of NGSIM data [54] is that this is *single-vehicle* data that allow us to study *microscopic* spatiotemporal empirical features of synchronized flow. Because of very expensive measurements, the data are measured at a very short road section only in a vicinity of on- and off-ramp bottlenecks on the road US 101 [Fig. 3(a)]. As explained in Ref. [58], we can assume that the NGSIM data can be associated with a (probably small) part of an expanded congested pattern (EP) measured by video cameras installed on a 640 m section of the road. In the data example (Fig. 3), there are time intervals in which moving jams exist in synchronized flow (bold vehicle trajectories 1, 4, and 5). These time intervals are intermediate with time intervals in which synchronized flow of low speed exists, in which no moving jams emerge (bold trajectories 2 and 3).

In numerical simulations we have found that at a given set of the flow rates on the main road, on-ramp inflows, and off-ramp outflows as well as at other given traffic parameters *arbitrary spatiotemporal transformations* between diverse congested patterns are possible to simulate in traffic flow of identical drivers [56] when the drivers choose different space gaps within the 2D region of synchronized flow states.

To demonstrate this conclusion of many simulations made in this work, we discuss in more detail one simulation scenario for a road section with five on ramp and five off ramps (Fig. 4). In the scenario there are two 20-minute-long time intervals 1 and 2. During time interval 1, all drivers entering the main road and on ramps choose space gaps in accordance with probabilities p_2 and p_1 from Table VII (see Appendix A) associated with "usual" (weak) speed adaptation. During time interval 2, all drivers entering the main road and on ramps

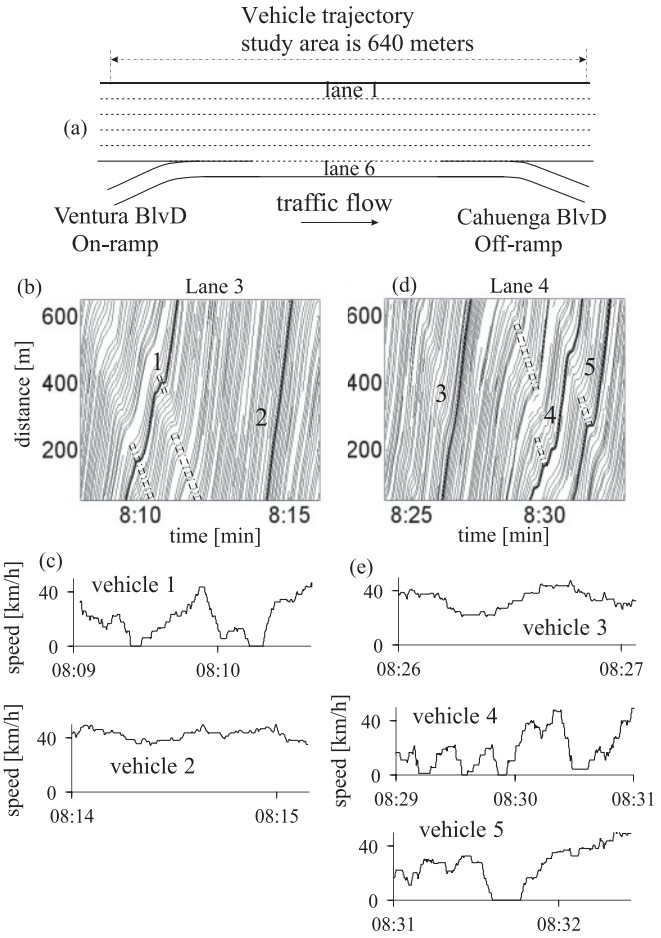

FIG. 3. Empirical spatiotemporal transformations between synchronized flow regions in which moving jams exist and synchronized flow regions without moving jams, which are reconstructed from single-vehicle data measured through video cameras installed on the road US 101 within 640 m section of the road US 101 shown in (a): Fragments of empirical vehicle trajectories (b), (d) and microscopic speeds along vehicle trajectories 1, 2 (c), and 3–5 (e) related to (b) and (d), respectively. Moving jams in (b), (d) are marked off by dashed curves. In (b), (d), each third vehicle trajectory is shown. NGSIM-single vehicle data measured on 15 June 2005 on 640 m section of the road US 101 [54].

choose space gaps in accordance with

$$p_2 = 1, \quad p_1 = 0.7 \tag{2}$$

associated with strong speed adaptation. At the beginning of the road and for each of the on ramps, the alternation of time intervals 1 and 2 is generated randomly with probability 0.5 for each of the intervals.

We find a very complex congested pattern within which two qualitatively different spatiotemporal regions can be distinguished, which are randomly distributed within the pattern (Fig. 4): regions in which moving jams propagate in synchronized flow [regions labeled as GP in Fig. 4(a), left] and regions of synchronized flow without the jams (labeled as SP). Spatiotemporal transformations from a GP region to SP region and back from a SP region to GP region occurring over time are shown in pattern fragments for microscopic

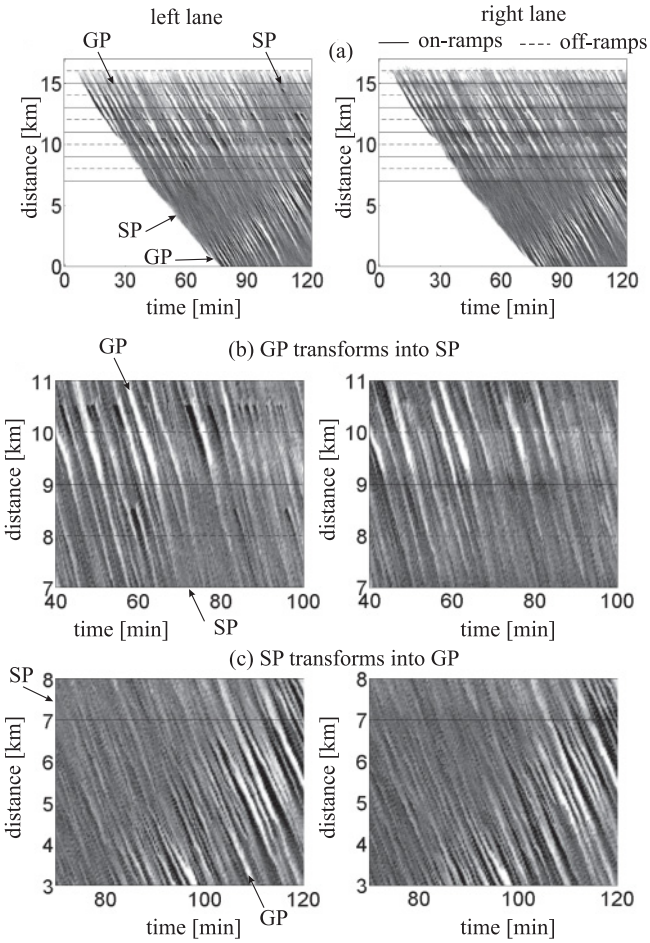

FIG. 4. Simulated random spatiotemporal transformations between SP regions and GP regions within a complex congested pattern: (a) Overview. (b), (c) Fragments within (a). Single-vehicle speed data presented by regions with variable shades of gray in space and time (in white regions the speed is higher than 25 km/h, in black regions the speed is zero). Simulation scenario is described in text. Beginning of merging regions of the on ramps and off ramps are at locations $x_{\text{on, i}} =$ 7, 9, 11, 13, 15 km and $x_{\text{off, j}} = 8$, 10, 12, 14, 16 km, respectively. Flow rates to on ramps $q_{\text{on i}}$, $i = 1, \ldots, 5$ and percentage of vehicles leaving the main road to off ramps η_j, $j = 1, \ldots, 5$ are $q_{\text{on i}} =$ 500, 400, 600, 720, 600 vehicles/h for $i = 1,2,3,4,5$, respectively; $\eta_j =$ 3%, 15%, 10%, 2%, 70% for $j = 1,2,3,4,5$, respectively. $q_{\text{in}} =$ 1500 (vehicles/h)/lane.

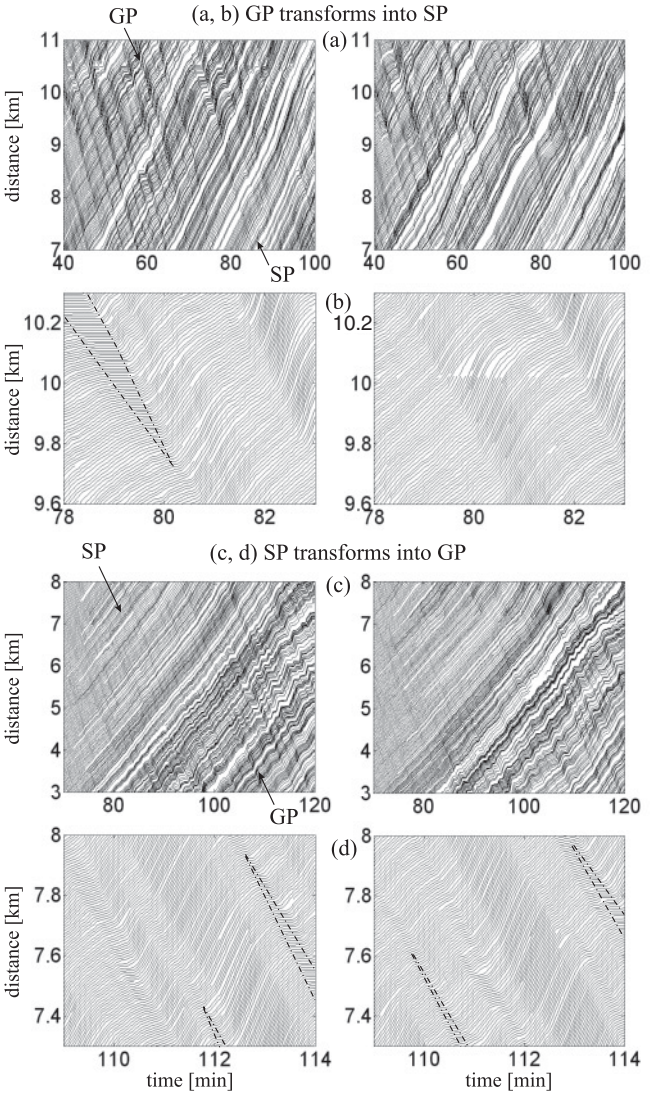

FIG. 5. Fragments of vehicle trajectories within the complex congested pattern shown in Fig. 4. Moving jams in (b), (d) are marked off by dashed curves.

speeds in Figs. 4(b) and 4(c), respectively. For more clarity, the same transformations are shown through vehicle trajectories in Figs. 5(a) and 5(c), respectively.

At a boundary separating GP and SP regions, the jam width (in the longitudinal direction) decreases, and all jams dissolve [Fig. 5(b)]. In contrast, at a boundary separating SP and GP regions, jams emerge spontaneously in synchronized flow, and their widths increase over time [Fig. 5(d)].

To prove that the moving jams in a GP region are wide moving jams and, therefore, the region is indeed associated with an GP, we presented single-vehicle speeds and time headways at time functions measured within the congested pattern via virtual detectors at two road locations, 9.5 and 7.5 km (Fig. 6). To distinguish wide moving jams and synchronized flow, we use the microscopic criterion for the wide moving jam phase [60,61]:

$$I_{\text{s}} = \frac{\tau_{\max}}{\tau^{(\text{a})}_{\text{del, jam}}} \gg 1, \tag{3}$$

where $\tau_{\max}$ is the maximum time headway that characterizes a so-called *flow interruption interval* within a wide moving jam; $\tau^{(\text{a})}_{\text{del, jam}}$ is the mean driver time delay in acceleration at the downstream front of the jam; in the model $\tau^{(\text{a})}_{\text{del, jam}} \approx$ 1.74 s. If in single-vehicle data related to congested traffic a flow-interruption interval is observed for a very low (or zero) speed that satisfies (3), then the related flow-interruption interval corresponds to the wide moving jam phase. After all wide moving jams have been found through this criterion in congested traffic, all remaining congested states are related to the synchronized flow phase.

At time $t \lesssim 82$ min, there are wide moving jams at location 9.5 km [Fig. 6(a)]: for some time headways at very low speeds the criterion (3) is satisfied [see Fig. 6(a), e.g., $\tau_{\max} \approx 14$ s

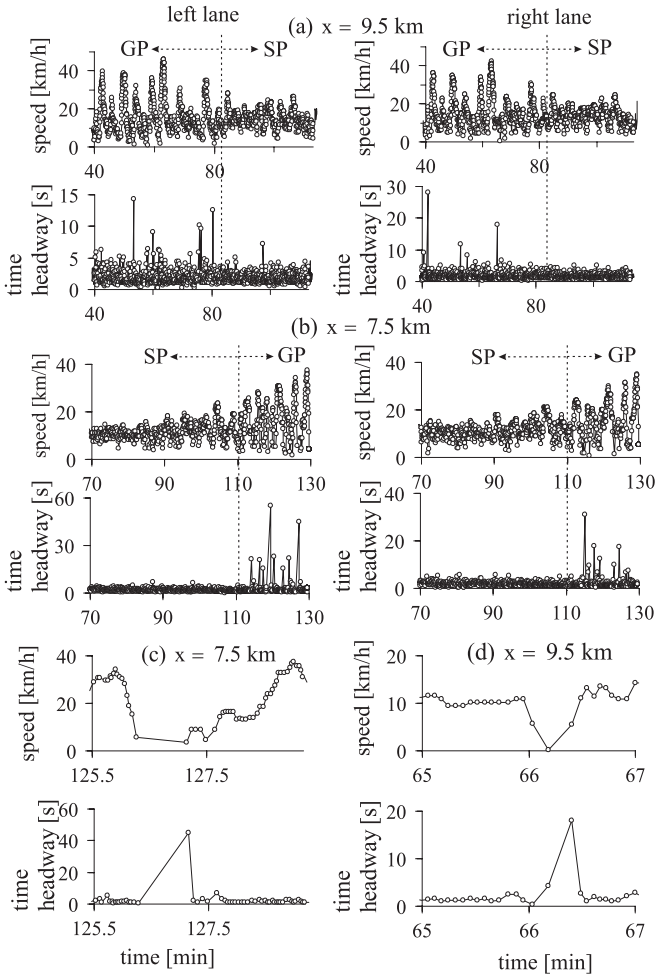

FIG. 6. Simulated single-vehicle speeds and time headways as time functions measured by two virtual detectors located at 7.5 and 9.5 km within the complex congested pattern shown in Fig. 4. Left and right figures are related to the left and right lanes, respectively.

and 28 s for two different wide moving jams in the left and right lanes, respectively]. In contrast, at time $t > 85$ min none of the time headways for low speeds satisfies (3); i.e., congested traffic is associated with synchronized flow only. In other words, at location 9.5 km a GP region transforms over time into a SP region at time $t \approx 82$ min. Because the mean synchronized flow speed between the jams within the GP region is higher than the one within the SP region, in Fig. 6(a) microscopic speed oscillations decrease in their amplitude at time $t \approx 82$ min.

In contrast, at location 7.5 km at time $t \approx 110$ min a SP region transforms over time into a GP region [Fig. 6(b)]. Indeed, at time $t \lesssim 110$ min there are no wide moving jams within synchronized flow, whereas at time $t > 112$ min many wide moving jams appear. This can be seen from time headways for low synchronized flow speeds: at $t \lesssim 110$ min for none of time headways criterion (3) is satisfied, whereas at $t > 112$ min there are many time headways for which criterion (3) is satisfied. Due to the transformation of the SP region into a GP one, speed oscillations increase over time considerably [Fig. 6(b)].

To prove the above application of criterion (3), in Figs. 6(c) and 6(d) we present two different time intervals in a considerably larger scale for two road locations, 7.5 and 9.5 km: we can see that low speeds satisfy criterion (3); i.e., within these time intervals wide moving jams have indeed been registered by virtual detectors at the locations.

The physics of arbitrary spatiotemporal transformations between GP and SP regions within congested patterns is the subject of Sec. III.

B. Interruption of jam growth in synchronized flow

In addition to random spatiotemporal transformations between complex GP and SP regions within traffic congestion (Sec. II A), a driver's arbitrary choice of a space gap within the 2D region of synchronized flow can explain the interruption of the jam growth leading to subsequent jam dissolution in synchronized flow occurring without any influence of lane changing [62]. Such interruption-nucleation effects in synchronized flow are observed in NGSIM-single-vehicle data (Sec. II B 1) and simulations (Sec. II B 2).

1. *Jam growth interruption in microscopic empirical data*

Empirical examples of the interruption of the jam growth leading to the subsequent jam dissolution in synchronized flow, which occur without lane changing, are shown in Figs. 7(a)–7(e).

In Fig. 7(a) can be seen two moving jams. Both jams have emerged within synchronized flow of low speed (Fig. 8). The space gap between vehicles labeled by numbers 1 and 2 (marked by bold trajectories) increases when vehicle 2 approaches the downstream jam, resulting in the decreasing in the jam width (in the longitudinal direction); that is, the jam growth is interrupted. However, the space gaps between vehicles 2 and 3 as well as 3 and 4 are considerably larger than between vehicles 1 and 2. This results in the subsequent full dissolution of both jams.

A qualitatively similar example is shown in Fig. 7(b). The jam growth interruption with subsequent jam dissolution correlates with a large space gap between two vehicles 5 and 6; these effects for another moving jam propagating later also correlate with the increase in space gaps between vehicles 7–10. The interruption of the jam growth with the subsequent jam dissolution in synchronized flow can also be seen in the microscopic speed distributions along vehicle trajectories shown in Fig. 8.

More complex empirical effects of the interruption of the jam growth are shown in Figs. 7(c)–7(e). In these cases, there are some time intervals between the interruption of the jam growth and subsequent jam dissolution. The time intervals can be explained through a complex distribution in space gaps between several vehicles (marked by bold trajectories) reaching the associated moving jams.

2. *Simulations of jam growth interruption in traffic flow of identical drivers*

Even for a given set of probabilities p_1 and p_2 for driver's speed adaptation, there can be a considerable difference in space gaps between vehicles. This is due to a stochastic

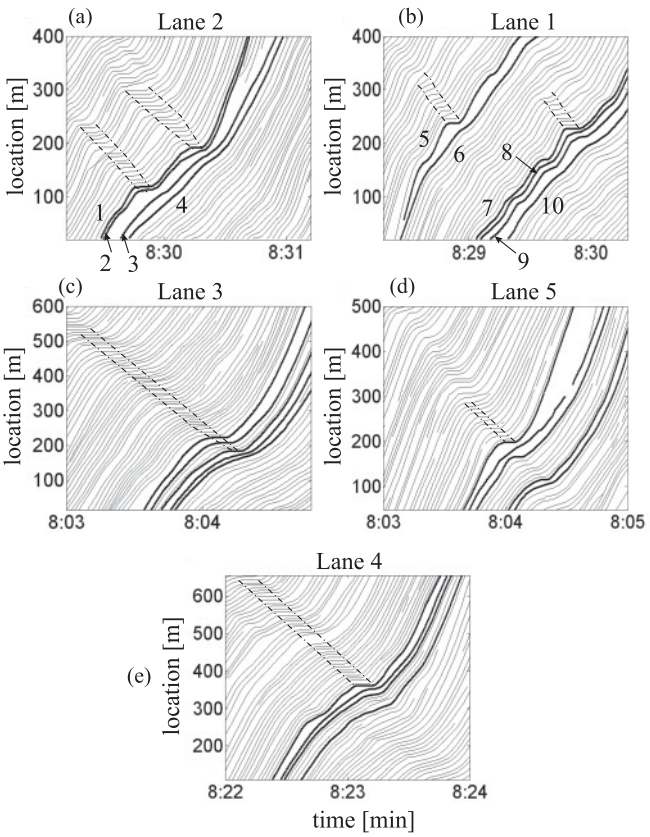

FIG. 7. Fragments of empirical vehicle trajectories reconstructed from single-vehicle data measured by video cameras installed on the road US 101 within a 640 m section of US 101 shown in Fig. 3(a). Moving jams are marked off by dashed curves. NGSIM-single-vehicle data measured on 15 June 2005 [54].

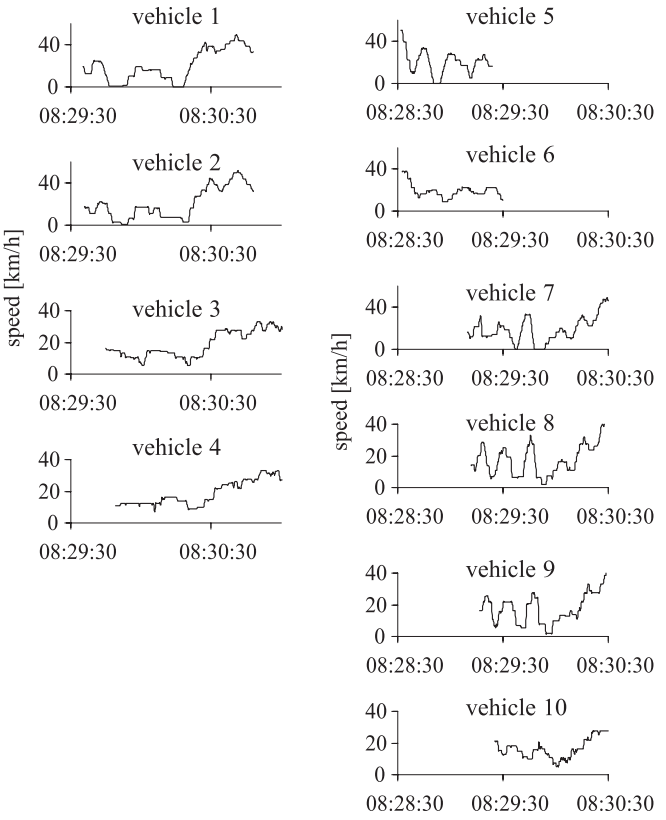

FIG. 8. Empirical microscopic vehicle speeds (in km/h) along vehicle trajectories 1–10 marked in bold in Figs. 7(a) and 7(b).

description of the driver's speed adaptation within the 2D region of synchronized flow made in the model (Appendix B). This explains simulation results of the interruption of the jam growth with subsequent jam dissolution associated with a random increase in a space gap between two vehicles reaching the jam (Fig. 9) calculated for p_1 and p_2 in Table VII. This interruption of the jam growth is responsible for jam dissolution in the left lane [labeled "jam" in Fig. 9(a)] as seen in vehicle trajectories [Fig. 9(b)].

In traffic flow of identical drivers in which drivers choose very different space gaps within the 2D region of synchronized flow, we have found a very complex jam dynamics with many nucleation-interruption effects that occur without lane changing. A simulation example presented in Figs. 10(b)–10(d) is made for a simulation scenario in which a complex EP occurs on a road section with five on-ramp and five off-ramp bottlenecks [Fig. 10(a)]. In the scenario 80% of drivers choose randomly space gaps associated with p_1 and p_2 in Table VII associated with weak speed adaptation, and 20% of drivers choose randomly greater space gaps within the 2D region of synchronized flow states associated with strong speed adaptation under conditions (2). The interruption of the jam growth with subsequent jam dissolution occurring in fragments of vehicle trajectories [Figs. 10(b)–10(d)] is due to the large difference in space gaps between drivers reaching the jam each after another.

It must be noted that real traffic does not usually consist of identical drivers and vehicles; that is, in real traffic flow there can be a mixture of trucks and cars driven by different drivers. In other words, we cannot state that in empirical data of complex traffic flow presented in Figs. 3, 7, and 8, vehicles

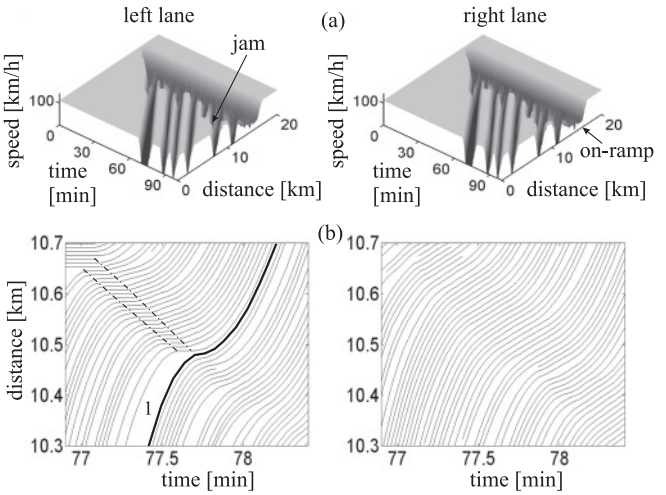

FIG. 9. Simulated speed within GP at on-ramp bottleneck (a) and a fragment of vehicle trajectories (b) within the GP. Left and right figures are related to the left and right lanes, respectively. All drivers choose space gaps associated with with p_1 and p_2 in Table VII. Moving jam is marked by dashed curves. $(q_{in},q_{on}) = (2000,900)$ [(vehicles/h)/lane, vehicles/h].

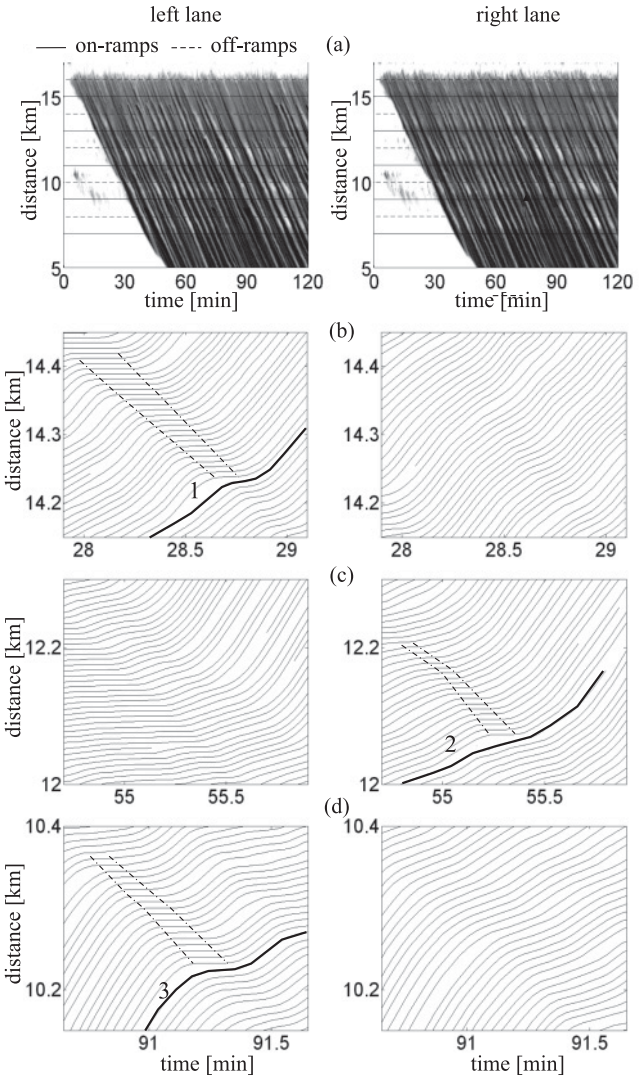

FIG. 10. Simulated speed within EP (a) and fragments of vehicle trajectories (b)–(d) within the EP in the left (left) and right (right) lanes. Drivers associated with p_1 and p_2 in Table VII (80%) and with Eq. (2) (20%) are distributed randomly in traffic flow. Moving jams in (b)–(d) are marked by dashed curves. Other model parameters are the same as those in Fig. 4.

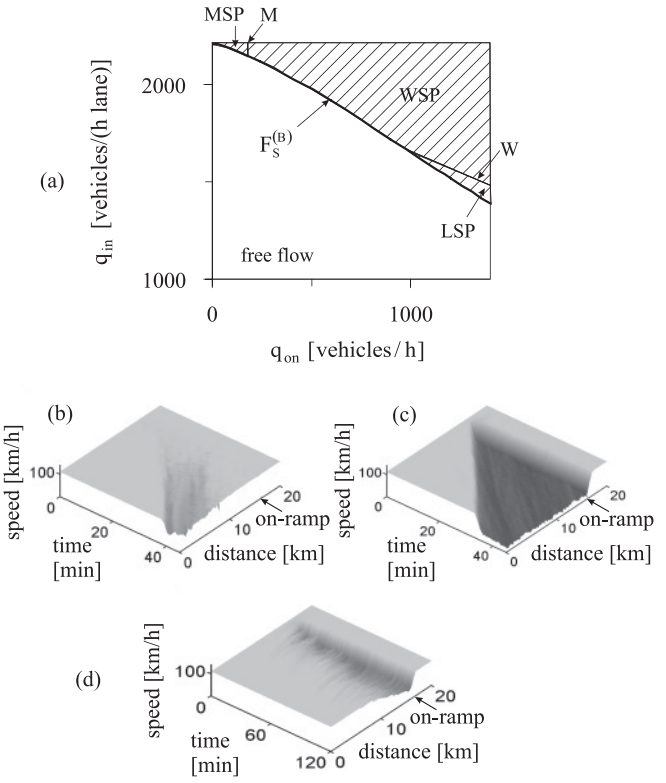

FIG. 11. Simulated synchronized flow patterns (SP) at on-ramp bottleneck under speed adaptation given by Eq. (4): (a) Diagram of congested patterns at on-ramp bottleneck. (b)–(d) Speed in space and time in the left lane within moving SP (MSP) (b), widening SP (WSP) (c), and localized SP (LSP) (d). $(q_{in},q_{on}) = (2118,30)$ (b), (2105,1400) (c), (1600,1000) (d) [(vehicles/h)/lane, vehicles/h]. In (a) line M separates MSPs (left to the line) and WSPs (right); line W separates WSPs (above the line) and LSPs (below) in the diagram.

are all the same. The main statement made above from a comparison of the empirical data and numerical simulations is that the empirical complexity of traffic flow can be simulated with a three-phase traffic flow model that incorporates the fundamental hypothesis of three-phase theory, *even* if in the simulations drivers and vehicles are all the same.

III. PHYSICS OF THE EFFECT OF FUNDAMENTAL HYPOTHESIS ON SPATIOTEMPORAL TRAFFIC PHENOMENA

To understand the physics of the complexity of spatiotemporal traffic phenomena in the flow of identical drivers revealed in Sec. II, we study separately congested patterns that occur at highway bottlenecks, when *only one* of the following three sets of speed adaptation parameters is used: Parameters of speed adaptation p_1 and p_2 are taken either from Table VII associated with "usual" (weak) speed adaptation, or from Eq. (2), or else from

$$p_2 = 1, \quad p_1 = 0.5. \tag{4}$$

Speed adaptation parameters given by Eq. (2) or by Eq. (4) are associated with strong speed adaptation. A subsequent comparison of features of congested patterns occurring for these three different sets of speed adaptation parameters p_1 and p_2 help us to disclose the physics of the fundamental hypothesis of three-phase theory in the description of spatiotemporal traffic phenomena.

A. Suppressing of emergence of wide moving jams in synchronized flow

The main effect of strong driver's speed adaptation within the 2D region of synchronized flow states is the suppression of the emergence of wide moving jams in synchronized flow. This can be seen when we compare the diagram of congested patterns at an on-ramp bottleneck for a driver's choice of space gap associated with parameters p_1 and p_2 in Table VII used in Fig. 2(c) [5,6] with the diagram found here [Fig. 11(a)] for a

driver's choice of space gap associated with speed adaptation parameters (4).

We have found that after an SP emerges at the flow rates q_{on} and q_{in} associated with the diagram boundary $F_S^{(B)}$ and then the on-ramp inflow rate q_{on} increases subsequently *no* wide moving jams emerge spontaneously in synchronized flow of the SP. This means that GPs do not appear even at low speeds and great vehicle densities within synchronized flow of the SP [Fig. 11(c)].

It must be mentioned that the degree of driver's speed adaptation associated with stochastic model parameters p_1 and p_2 is *not* a driver characteristic that describes a particular driver: The fundamental hypothesis states that the arbitrary space gap choice within the 2D region of synchronized flow can be made by any driver [63]. In other words, within the 2D region of synchronized flow, a driver can freely choose the degree of driver's speed adaptation (stronger or weaker adaptation) and change freely this speed adaptation degree over time. Thus the suppression of wide moving jam emergence in synchronized flow under strong speed adaptation (4) (Fig. 11) occurs under the condition that *all* driver behavioral characteristics, which characterize different drivers in relation to their reaction times and other safety driver abilities, remain the same as those used in Fig. 2(c) [5,6] (Table VII). In particular, all drivers exhibit the same reaction time, safe speed, and slow-to-start rule [56,64] that is responsible for wide moving jam propagation [65] (see Sec. III E).

B. Drivers' choice of space gap and line *J*

If under condition (B1) of Appendix B drivers choose the space gap in accordance with p_1 and p_2 of Table VII, synchronized flow states within an WSP [Fig. 12(a)] lie above the line J in the flow-density plane [circle points in Fig. 12(b)]. These synchronized flow states are metastable with respect to wide moving jam emergence [66]. This explains why the WSP [Fig. 12(a)] transforms spontaneously into an GP like that shown in Fig. 2(b), when the flow rates increase and a point (q_{on},q_{in}) lies right to the boundary $S_J^{(B)}$ in Fig. 2(c).

In contrast, for strong driver's speed adaptation (4), synchronized flow states within an WSP [Fig. 12(c)] lie on and below the line J in the flow-density plane [circle points in Fig. 12(d)]. Because synchronized flow states below the line J are stable with respect to the jam emergence [66] and in synchronized flow states lying on the line J only a very great disturbance (like a long stop of one of the vehicles) in synchronized flow can lead to the jam emergence [5], no wide moving jams emerge spontaneously under condition (4). Under more stronger speed adaptation (2), synchronized flow points in the flow-density plane move below the line J [circle points in Fig. 12(f)]; i.e., all synchronized flow states within an WSP [Fig. 12(e)] are stable with respect to the jam emergence [66].

Driver's choice of strong speed adaptation [conditions (2) or (4)] leads to a quicker vehicle deceleration to the speed of the preceding vehicle, that is, to a larger space gap (longer time headway) at which the vehicle follows the preceding vehicle [67]. However, at a given speed the larger the gap, the more stable the synchronized flow with respect to wide moving jam emergence [3,5,66].

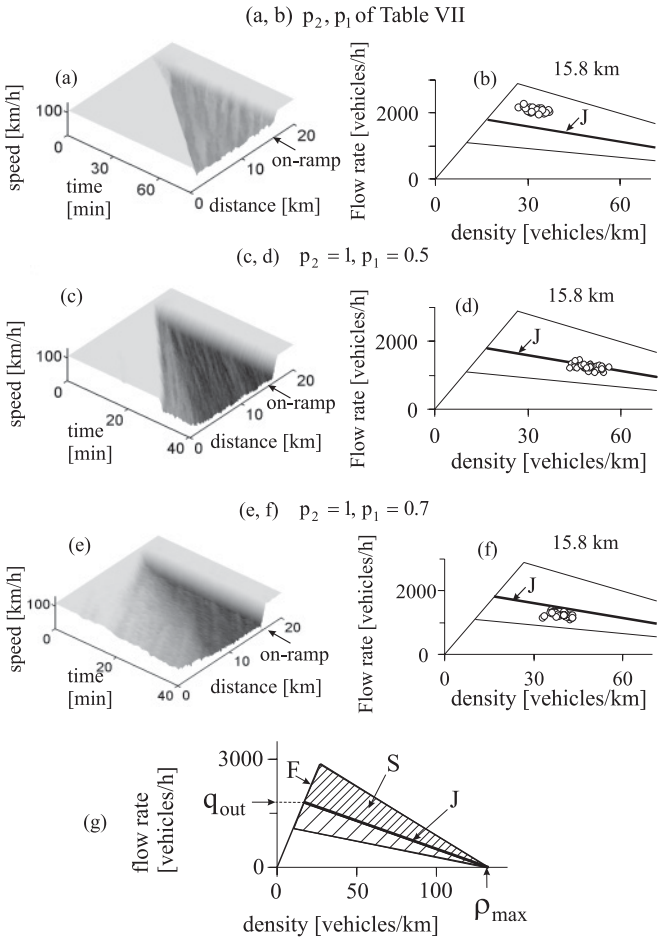

FIG. 12. Explanation of the physics of the effect of the fundamental hypothesis of three-phase theory on congested patterns: (a), (b) Speed in space and time in the left road lane within WSP at on-ramp bottleneck (a) and related points (circles associated with 1-min average data) for synchronized flow within the WSP at location 15.8 km in the flow-density plane (b) for speed adaptation used in Refs. [58,59] and given in Table VII. (c)–(f) Speed in space and time in the left lane within WSPs at on-ramp bottleneck (c), (e) and related points (circles) for synchronized flow within the WSPs (d), (f) under stronger speed adaptation given by (4) (c), (d) and by (2) (e), (f). $(q_{in},q_{on}) = (2250,240)$ (a),(b) and (2100,1400) (c)–(f) [(vehicles/h)/lane, vehicles/h]. (g) Explanation of 2D region of synchronized flow and line J.

C. Traffic breakdown and infinite number of highway capacities

Although under strong speed adaptation (4) no wide moving jams emerge spontaneously in synchronized flow, traffic breakdown remains a first-order F → S transition. This conclusion can be drawn from results presented in Fig. 13.

We have found that traffic breakdown at the bottleneck can be either spontaneous [Fig. 13(a)–13(c)] or induced [Fig. 13(d)]. After the on-ramp inflow has been switched on, the spontaneous traffic breakdown occurs with a random time delay $T_{FS}^{(B)}$ [Fig. 13(a)–13(c)]. The time delay of traffic breakdown $T_{FS}^{(B)}$ is a random value: In different simulation realizations (runs), which have been made at the same flow rates and other model parameters but at different initial

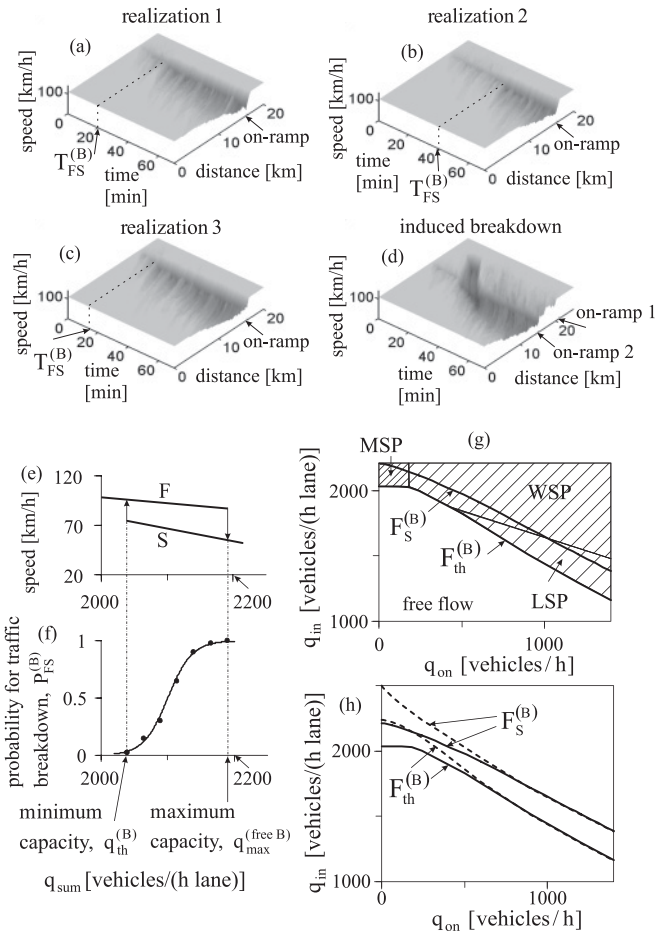

FIG. 13. Features of traffic breakdown under driver's strong speed adaptation (4): (a)–(c) Speed in the right lane during spontaneous traffic breakdown at on-ramp bottleneck in three simulation realizations (runs) at $(q_{in},q_{on}) = (1715,900)$ (vehicles/h)/lane, vehicles/h; $T_{FS}^{(B)} = 20$ (a), 38 (b), and 14 min (c). (d) Induced traffic breakdown: SP at downstream on ramp 1 located at 21 km is induced through a time-limited increase in q_{on1} from 60 to 1000 vehicles/h between $t =$ 5 and 15 min; while reaching the upstream on ramp 2 at 15 km, the SP induces WSP at this on-ramp bottleneck; $(q_{in},q_{on2}) = (1715,900)$ [(vehicles/h)/lane, vehicles/h]. (e), (f) Z characteristic for traffic breakdown (F, free flow; S, synchronized flow) (e) and the probability of traffic breakdown as a function of the flow rate downstream of the bottleneck q_{sum} (where $q_{sum} = q_{in} + 0.5q_{on}$) (f) for $T_{ob} = 30$ min at $q_{in} = 1715$ (vehicles/h)/lane. (g) Full diagram of congested patterns at the on-ramp bottleneck with the threshold boundary for traffic breakdown $F_{th}^{(B)}$. (h) Comparison of diagram boundaries $F_S^{(B)}$, $F_{th}^{(B)}$ under speed adaptation parameters of (4) [solid curves taken from (g)] and of Table VII (dashed curves).

conditions for model fluctuations, we have found different $T_{FS}^{(B)}$ [Figs. 13(a)–13(c)].

In accordance with three-phase theory [5], there are the infinite number of highway capacities. Recall that a highway capacity q_C of free flow at a bottleneck is defined as the flow rate at the bottleneck q_{sum} at which traffic breakdown can occur at the bottleneck with probability $P_{FS}^{(B)} > 0$. Each of the capacities exhibits two attributes: the breakdown probability $P_{FS}^{(B)}$ and the observation time for traffic variables T_{ob}. The infinite number of highway capacities $q_{sum} = q_C$ are within the flow rate range [Figs. 13(e) and 13(f)] [5,68,69]

$$q_{th}^{(B)} \leqslant q_{sum} \leqslant q_{max}^{(free\,B)}, \tag{5}$$

where $q_{th}^{(B)}$ is a threshold flow rate that determines the minimum capacity: at $q_{sum} < q_{th}^{(B)}$ during the interval T_{ob} the breakdown probability $P_{FS}^{(B)} = 0$; $q_{max}^{(free\,B)}$ is the maximum flow rate that determines the maximum capacity; at $q_{sum} = q_{max}^{(free\,B)}$ the breakdown probability $P_{FS}^{(B)} = 1$.

The infinite number of highway capacities are explained by the metastability of free flow with respect to traffic breakdown (F $\rightarrow$ S transition). The free flow metastability to the breakdown is clearly seen on a Z characteristic for traffic breakdown calculated for a given q_{in} and varying q_{on} in Fig. 13(e).

The metastablity of free flow for strong speed adaptation (4) can also be clearly seen in the diagram of congested patterns if to the diagram shown in Fig. 11(a) a threshold boundary for traffic breakdown $F_{th}^{(B)}$ is added [Fig. 13(g)]: Free flow is metastable with respect to traffic breakdown between the boundary $F_S^{(B)}$, at which the probability of traffic breakdown during the time interval T_{ob} reaches 1, and the threshold boundary $F_{th}^{(B)}$: Left to and below the threshold boundary the probability of traffic breakdown during this time interval is zero. For the diagrams of congested patterns at the on-ramp bottleneck shown in Figs. 13(g) and 13(h), the flow rate $q_{sum} = q_{in} + 0.5q_{on}$, and, therefore, a function $q_{th}^{(B)}(q_{on}) - 0.5q_{on}$ gives the boundary $F_{th}^{(B)}$, whereas a function $q_{max}^{(free\,B)}(q_{on}) - 0.5q_{on}$ gives the boundary $F_S^{(B)}$.

For small on-ramp inflows q_{on}, diagram boundaries $F_S^{(B)}$, $F_{th}^{(B)}$ under strong speed adaptation (4) [solid curves in Fig. 13(h)] are below the associated diagram boundaries calculated under speed adaptation parameters in Table VII [dashed curves in Fig. 13(h)]. However, when q_{on} increases, the associated boundaries approach each other. In other words, at small q_{on} the maximum capacity $q_{max}^{(free\,B)}$ under strong speed adaptation (4) is smaller than the one for parameters in Table VII; the same result is valid for the minimum capacity $q_{th}^{(B)}$. The larger the on-ramp inflow, the smaller the difference between maximum capacities and the difference between minimum capacities for strong and weak speed adaptations [Fig. 13(h)].

A qualitative explanation of this result is as follows: The stronger the driver's speed adaptation within the 2D region of synchronized flow states, the easier the formation of synchronized flow; therefore, both maximum and minimum capacities decrease. The increase in on-ramp inflow q_{on} leads to the increase in the frequency of nucleus occurrence required for the breakdown that determines mostly the breakdown probability. This may explain the above result that at larger q_{on} the maximum and minimum capacities do not almost depend on the degree of driver's speed adaptation.

D. Transformation of GP into SP

When a point (q_{on},q_{in}) in the diagram of congested patterns is right of the boundary $S_J^{(B)}$ [Fig. 2(c)], an GP occurs spontaneously [Fig. 14(a)] at weak speed adaptation (p_1 and p_2 of Table VII). However, this GP transforms spontaneously into an SP [Fig. 14(c)], when drivers increase speed adaptation

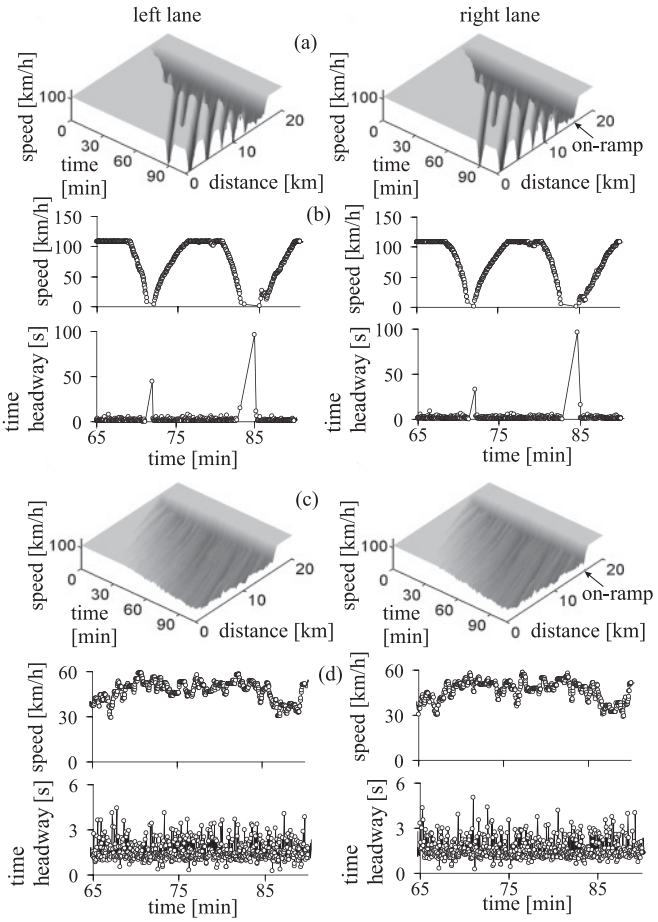

FIG. 14. Simulations of transformation of GP (a), (b) associated with diagram shown in Fig. 2(c) (model parameters of Table VII) into WSP (c), (d) associated with diagram shown in Fig. 11(a) through a driver's choice of stronger speed adaptation parameters (4) at given $q_{on} = 900$ vehicles/h and $q_{in} = 1850$ (vehicles/h)/lane: (a), (c) Speed in space and time. (b), (d) Single-vehicle speeds and time headways as time functions at location 10 km related to (a) and (c), respectively.

within the 2D region of synchronized flow states. This follows from a comparison of diagrams for congested patterns shown in Figs. 2(c) and 11(a) made in Sec. III A. Because upstream fronts of wide moving jams while propagating in traffic decrease traffic safety considerably, the effect of the transformation of the GP into SP can be useful for traffic control [70].

It should be mentioned that the transformation of the SP into GP shown in Fig. 2 and discussed in Sec. I is due to the associated increase in q_{on} or/and q_{in} that moves a point (q_{on}, q_{in}) in the diagram of congested patterns right to the boundary $S_J^{(B)}$. In contrast, in the case under consideration (Fig. 14) the transformation of the GP into SP occurs at *given flow rates* q_{on}, q_{in} through a change in the driver's choice of space gaps under condition (B1) of Appendix B. Through this pattern transformation, microscopic traffic flow characteristics change considerably: Long flow interruption intervals within wide moving jams [Fig. 14(b)] that satisfy microscopic jam criterion (3) are replaced by short time headways [Fig. 14(d)] that do not satisfy (3) associated with synchronized flow in which no wide moving jams occur.

A very great bottleneck strength can be reached at a sequence of closely located adjacent on- and off-ramp bottlenecks leading to a very low speed in synchronized flow. In particular, at the sequence of five on-ramp and five off-ramp bottlenecks for flow in which all drivers choose weak speed adaptation associated with parameters of Table VII a very complex expanded GP (EGP) can appear [Fig. 15(a)] [58]. The EGP [Fig. 15(a)] transforms into an expanded SP (ESP) [Fig. 15(d)] if all drivers choose strong speed adaptation (4). It must be mentioned that both the EGP [Fig. 15(a)] and ESP [Fig. 15(d)] are simulated at the same flow rates to on and off ramps and on the main road as well as for the same set of the bottlenecks. As in the case of the transformation of the GP into SP at a single bottleneck (Fig. 14), the transformation of the EGP into ESP causes the dissolution of long flow interruption intervals associated with wide moving jams of the EGP [Fig. 15(c)]; the jam dissolution results in short time headways [Fig. 15(f)] that do not satisfy (3): Synchronized flow of a very low speed occurs within the ESP [Fig. 15(e)] in which no wide moving jams emerge spontaneously.

E. Induced emergence of wide moving jam and its propagation

Although wide moving jams do not emerge spontaneously within synchronized flow under strong driver's speed adaptation (Secs. III A–III D), a wide moving jam (s) can be induced in synchronized flow. To study the propagation of a wide moving jam through synchronized flow at different driver's choices of space gaps within the 2D region of synchronized flow states, a wide moving jam has been induced downstream of SPs [Figs. 16(a), 16(c), and 16(d)].

While propagating through synchronized flow the wide moving jam maintains the mean velocity of the jam downstream front independent of the degree of speed adaptation chosen by drivers; i.e., in all cases [Figs. 16(a), 16(c), and 16(d)] the downstream jam front is associated with the line J in the flow-density plane [Figs. 16(b) and 16(e)]. However, when drivers choose strong speed adaptation (4) [Figs. 16(a) and 16(c)], the absolute value of the velocity of the upstream jam front is smaller than that for the downstream jam front: respectively, the lines representing the propagation of the upstream jam fronts [line denoted by *up* in Fig. 16(b)] are below the line J. This is explained by the above result (Sec. III B) that under condition (4) many synchronized flow states within SPs are below the line J in the flow-density plane [Fig. 12(d)]. For this reason the absolute value of the downstream jam front velocity is higher then the one for the upstream jam front; therefore, in both cases the jam width (in the longitudinal direction) decreases over time, and the jam dissolves finally [Figs. 16(a) and 16(c)].

For a comparison with this jam dissolution, in Fig. 16(d) the well-known result [5] is shown that under "usual" driver's speed adaptation (Table VII) the jam width increases over time while the jam propagates through synchronized flow of the WSP. This jam growth is associated with the greater absolute value of the velocity of the upstream jam front [line *up* in Fig. 16(e)] than that for the downstream jam front (line J). This is explained by the above result (Sec. III B) that in the case most of synchronized flow states within SPs are above the line J in the flow-density plane [Fig. 12(b)]. For this reason,

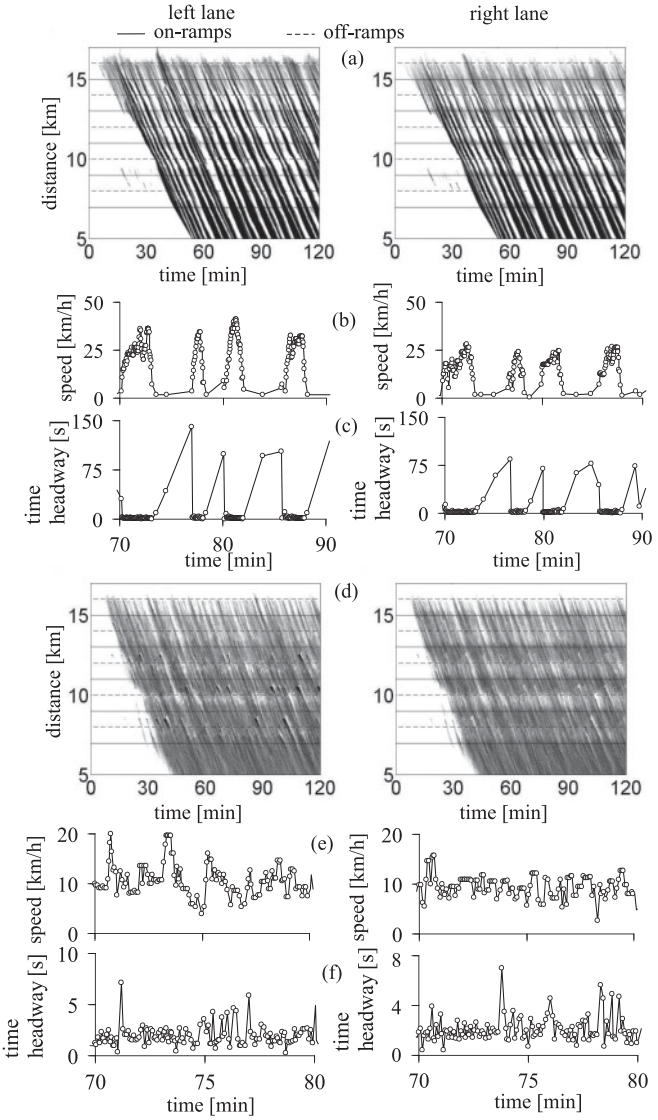

FIG. 15. Simulations of transformation of EGP (a)–(c) into expanded SP (ESP) (d)–(f) through the change in driver's choice in space gap within the 2D region of synchronized flow (figures left and right are related to the left and right lanes, respectively): (a), (d) Single-vehicle speed data for fragments within the EGP (a) and ESP (d) presented by regions with variable shades of gray in space and time (in white regions the speed is higher than 30 km/h; in black regions the speed is zero). (b), (c), (e), (f) Single-vehicle speeds (b), (e) and time headways (c), (f) measured within the EGP (a)–(c) and ESP (d)–(f) at location 7 km through the use of virtual detectors. Other model parameters are the same as those in Fig. 10.

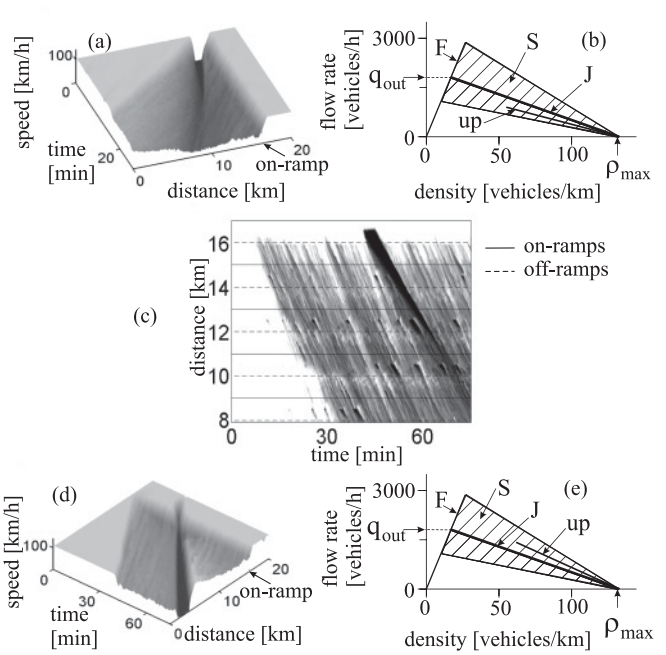

FIG. 16. Propagation of wide moving jam through three different SPs associated with synchronized flows in which drivers choose either strong speed adaptation (4) (a)–(c) or "usual" speed adaptation (Table VII) (d), (e): (a), (d) Average speed in space and time in the left lane for WSPs at on-ramp bottleneck located at 15 km. (c) Speed data presented by regions with variable shades of gray in space and time; ESP is the same as shown in Fig. 15(d). (b), (e) Steady states of synchronized flow S, line J for the downstream jam front, and lines denoted by up related to the upstream jam fronts for the jams shown in (a), (c), and (d), respectively. Model parameters for (a) and (c) are the same as those used in Figs. 12(c) and 15(d), respectively. In (d), $(q_{in},q_{on}) = (2100,650)$ [(vehicles/h)/lane, vehicles/h]. In (a), (c), (d), the jams have been induced by local time-limited disturbances created simultaneously in both lanes through the deceleration of one of the vehicles in each of the road lanes to the speed $v_{dis} = 0$; these vehicles have been in a standstill during a time interval $T_{dis} = 3$ min, and then the vehicles can accelerate freely.

the absolute value of the downstream jam front velocity is smaller then the one for the upstream jam front; therefore, the jam width increases over time [Fig. 16(d)].

IV. DISCUSSION

A. Random moving jam emergence in synchronized flow

Up to now we have considered the effect of the fundamental hypothesis of three-phase theory on spatiotemporal traffic phenomena through a comparison of features of synchronized flows of drivers choosing either weak (Table VII) or strong [(2) and (4)] speed adaptation in the 2D region of synchronized flow states. When drivers choose an intermediate degree of speed adaptation

$$p_2(v_n) = 0.8 + 0.2\Theta(v_n - v_{21}), \quad p_1 = 0.42, \qquad (6)$$

we have found that wide moving jams can spontaneously emerge in synchronized flow; however, the diagram boundary $S_J^{(B)}$ [Fig. 2(c)], at which with probability 1 a wide moving jam(s) emerges spontaneously in synchronized flow during the observation time interval $T_{ob,\,SJ} = 60$ min, moves to considerably greater values of the on-ramp inflow [Fig. 17(a)]. This allows us to distinguish in the diagram broad subregions with different probability of wide moving jams [labeled $S_J^{(B)}$ (probability 0.5) and $S_J^{(B)}$ (probability 0.1) in Fig. 17(a)]: In some of the simulation runs, an SP remains; however, in the other ones the SP transforms into an GP [71]. This random jam emergence is illustrated for (q_{in},q_{on}) related to points A and B in the diagram [Fig. 17(a)]: In some of the realizations, WSPs

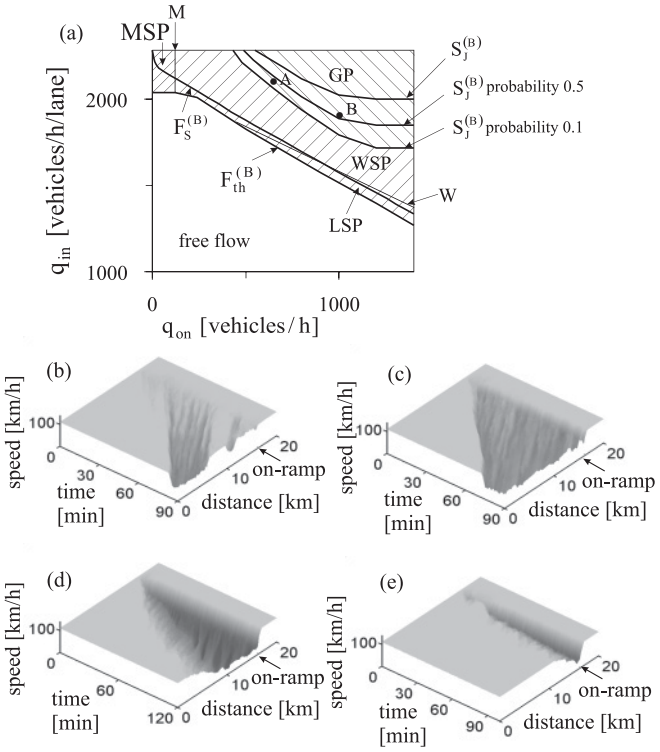

FIG. 17. Diagram of congested patterns at on-ramp bottleneck under condition (6) (a) and related SPs: (b)–(e) Speed in space and time in the left lane for MSP (b), WSP (c), (d), LSP (e) at $(q_{in},q_{on}) = (2250,90)$ (b), (2180,360) (c), (1850,900), (d), and (1630,1000) (e) [(vehicles/h)/lane, vehicles/h]. In (a), line M separates MSPs (left to the line) and WSPs (right); line W separates WSPs (above the line) and LSPs (below) in the diagram.

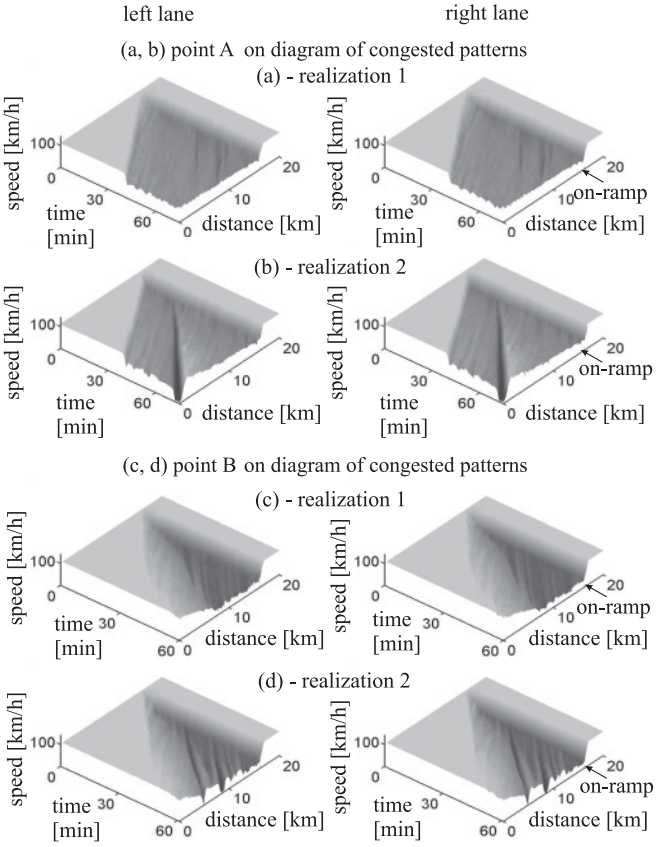

FIG. 18. Different realizations of congested patterns at on-ramp bottleneck under condition (6) related to points A (a), (b) and B (c), (d) on diagram of congested patterns shown in Fig. 17. $(q_{in},q_{on}) = (2100,650)$ (a), (b) and (1900,1000) (c), (d) [(vehicles/h)/lane, vehicles/h].

[Figs. 18(a) and 18(c)], however, in other ones, GPs appear [Figs. 18(b) and 18(d)].

In general, we have found that the stronger the driver's speed adaptation, the more the boundary $S_J^{(B)}$ moves to the right in the diagram, i.e., the greater the on-ramp inflow (bottleneck strength) at which wide moving jams emerge spontaneously in synchronized flow; finally, under strong enough speed adaptation (4) no wide moving jams emerge spontaneously at all bottleneck strengths that can be reached in our simulations.

The analysis made above shows that the stronger the speed adaptation chosen by drivers, the longer the mean time headway between vehicles within synchronized flow, i.e., the larger the mean space gap between vehicles. For "usual" speed adaptation parameters (Table VII) and strong speed adaptation parameters given by (4) and (2), the mean space gaps (mean time headways) within the related WSPs are, respectively, 15 m (1.6 s) [Figs. 12(a) and 12(b)], 25 m (1.78 s) [Figs. 12(c) and 12(d)], and 30 m (1.9 s) [Figs. 12(e) and 12(f)].

When the preceding vehicle decelerates unexpectedly, the larger mean space gap within synchronized flow is, the longer the time interval that a driver has on average to adapt the speed to the speed of the preceding vehicle at the same driver time delay in deceleration (at the same driver reaction time). This means that the larger mean space gap within synchronized flow, the smaller the probability of driver's over-deceleration (driver-over-reaction), i.e., the smaller the probability of driver's deceleration to a lower speed than the speed of the preceding vehicle (driver's over-deceleration). This explains the above result that the stronger the speed adaptation chosen by drivers, the smaller the probability of wide moving jam emergence in synchronized flow.

B. Fundamental hypothesis of three-phase theory as the result of traffic phase definitions

The fundamental hypothesis of three-phase theory [3] is the result of the empirical traffic phase definitions [J] and [S], as explained below.

The line J in the flow-density plane results from the definition of wide moving jam [J]. Any point on the line J can be a final steady traffic state for vehicles accelerating at the downstream front of a wide moving jam. If the speed in this state is lower than the minimum speed that is possible in free flow, the state is a synchronized flow steady state that lies on the line J. Thus there should be infinite synchronized flow states lying on the line J [Fig. 12(g)].

The definition of synchronized flow [S] means that downstream fronts of synchronized flow regions do *not* exhibit the jam characteristic feature [J]. For this reason, in addition to synchronized flow steady states lying on the line J, there should be synchronized flow steady states that are outside of the line J in the flow-density plane. Indeed, only in this case

does the downstream front between two different states of synchronized flow not exhibit the characteristic jam velocity given by the slope of the line J. Thus there should be also steady states of synchronized flow outside of the line J, i.e., there is a 2D region of the steady states in the flow-density plane. This explains the fundamental hypothesis of three-phase traffic theory about the 2D region of the steady states of synchronized flow [Fig. 12(g)].

The definition [S] is associated with empirical results for moving jam behavior within synchronized flow [5]: Depending on synchronized flow characteristics upstream of a moving jam, the jam can either grow or dissolve, propagating in the synchronized flow over time. We have noted that there are an infinite number of steady states of synchronized flow that lie on the line J. If these states were to build the upper boundary of the 2D region of the synchronized flow steady states, i.e., there were no steady states above the line J, then a wide moving jam should dissolve, propagating in the states of synchronized flow. This contradicts a possibility of the jam growth. In contrast, if the states on the line J were to build the low boundary of the 2D region of the synchronized flow steady states, i.e., there were no steady states below the line J, then no wide moving jam can dissolve, propagating in the states of synchronized flow. This also contradicts mentioned empirical results about possible jam dissolution. Thus we should assume that there are synchronized flow steady states above *and* below the line J [Fig. 12(g)].

C. Conclusions and outlook

The above study allows us to draw the following conclusions:

1. Macroscopic and microscopic spatiotemporal effects of the *entire complexity* of traffic congestion observed up to now in real measured traffic data can be explained by simulations of traffic flow consisting of *identical* drivers and vehicles, if a microscopic model used in these simulations incorporates the fundamental hypothesis of three-phase theory. This is due to the statement of the fundamental hypothesis about a driver's arbitrary choice of a space gap (time headway) within the 2D region of synchronized flow.

2. When drivers make over time another choice of space gaps (time headways) within the 2D region of synchronized flow, then at given flow rates and given other road and traffic parameters extremely complex pattern transformations can occur, like a pattern type changes qualitatively to another one or qualitative spatiotemporal characteristics of traffic congestion within a complex congested pattern change randomly.

3. The driver's choice of space gaps within the 2D region of synchronized flow associated with the fundamental hypothesis of three-phase theory can qualitatively change types of congested patterns that can emerge at a highway bottleneck as well as a diagram of congested patterns at the bottleneck. Independent of the pattern type at the bottleneck traffic congestion emerges spontaneously in an initial free flow at the bottleneck due to a first-order F $\rightarrow$ S transition.

4. We have found that if drivers choose long enough space gaps within the 2D region of synchronized flow associated with the fundamental hypothesis, then GPs do not emerge at the bottleneck independent of the flow rates and bottleneck characteristics. In this case we have derived the following particular results:

In the diagram of congested patterns at the bottleneck, a usually existing region of GPs can disappear fully; i.e., only SPs exist at the bottleneck at any flow rates.

At any flow rates at a heavy bottleneck, which leads to a very low speed within congested patterns at the bottleneck, only SPs occur in which no wide moving jams emerge spontaneously.

5. These results of the article emphasize the effect of the fundamental hypothesis on spatiotemporal traffic phenomena disclosing the physics of the hypothesis.

Naturally, simulations of a driver's arbitrary choice of a space gap with the use of stochastic driver's speed adaptation (model parameters p_1 and p_2 discussed in Appendix B) is a model simplification. However, this simple solution for the driver's gap choice made in the article has allowed us to disclose the physics behind the fundamental hypothesis of three-phase theory [53].

In reality, we can expect that sometimes a driver can choose the space gap within the 2D region of synchronized flow states in accordance with a particular driving situation as well as due to some collective effects, for example, while observing space gaps chosen by neighborhood drivers in synchronized flow. The development of new three-phase models that incorporate such individual and collective effects is a challenge for traffic flow theory.

ACKNOWLEDGMENT

I thank S. L. Klenov for discussions and help in simulations.

APPENDIX A: KERNER-KLENOV THREE-PHASE TRAFFIC FLOW MODEL AND MODEL PARAMETERS

In this Appendix a discrete version of the Kerner-Klenov stochastic three-phase traffic flow model [58,59] whose continuum version has initially been derived in Refs. [7,57] is presented. In the model a small enough value of the discretization cell δx is used. Consequently the vehicle speed

TABLE I. Functions model I: Model speed fluctuations.

$$\xi_n = \begin{cases} \xi_a & \text{if} \quad S_{n+1} = 1 \\ -\xi_b & \text{if} \quad S_{n+1} = -1 \\ \xi^{(0)} & \text{if} \quad S_{n+1} = 0, \end{cases}$$

S_{n+1} is the "state of vehicle motion" at time step $n+1$:

$$S_{n+1} = \begin{cases} -1 & \text{if} \quad \tilde{v}_{n+1} < v_n \\ 1 & \text{if} \quad \tilde{v}_{n+1} > v_n \\ 0 & \text{if} \quad \tilde{v}_{n+1} = v_n, \end{cases}$$

$$\xi_a = a^{(a)}\tau\Theta(p_a - r), \xi_b = a^{(b)}\tau\Theta(p_b - r),$$

$$\xi^{(0)} = a^{(0)}\tau \begin{cases} -1 & \text{if} \quad r \leqslant p^{(0)} \\ 1 & \text{if} \quad p^{(0)} < r \leqslant 2p^{(0)} \text{ and } v_n > 0 \\ 0 & \text{otherwise,} \end{cases}$$

$r = \text{rand}(0,1)$, $\Theta(z) = 0$ at $z < 0$ and $\Theta(z) = 1$ at $z \geqslant 0$;

$a^{(a)} = a^{(a)}(v_n)$, $a^{(b)} = a^{(b)}(v_n)$;

p_a, p_b, $p^{(0)}$, $a^{(0)}$ are constants.

TABLE II. Functions in model II: Stochastic time delay of acceleration and deceleration.

$$a_n = a\Theta(P_0 - r_1),\ b_n = a\Theta(P_1 - r_1),$$
$$P_0 = \begin{cases} p_0 & \text{if} \quad S_n \neq 1 \\ 1 & \text{if} \quad S_n = 1, \end{cases} \qquad P_1 = \begin{cases} p_1 & \text{if} \quad S_n \neq -1 \\ p_2 & \text{if} \quad S_n = -1, \end{cases}$$
$r_1 = \text{rand}(0,1)$, $\Theta(z) = 0$ at $z < 0$ and $\Theta(z) = 1$ at $z \geqslant 0$,
$p_0 = p_0(v_n)$,
$p_2 = p_2(v_n)$, p_1 is constant.

and acceleration (deceleration) discretization intervals are $\delta v = \delta x/\tau$ and $\delta a = \delta v/\tau$, respectively, where time step $\tau = 1$ s. Because in the discrete model version discretized (and dimensionless) speed and acceleration are used, which are measured respectively in the discretization values δv and δa, time step τ in all formulas below is assumed to be the dimensionless value $\tau = 1$. Explanations of the physics of vehicle motion rules in this model can be found in Sec. 16.3 of Ref. [5]. The model for a two-lane road reads as follows [58,59]:

$$v_{n+1} = \max\,(0,\ \min(v_{\text{free}},\ \tilde{v}_{n+1} + \xi_n, v_n + a\tau, v_{s,n})), \tag{A1}$$

$$x_{n+1} = x_n + v_{n+1}\tau, \tag{A2}$$

$$\tilde{v}_{n+1} = \max\,(0,\ \min(v_{\text{free}}, v_{s,n}, v_{c,n})), \tag{A3}$$

$$v_{c,n} = \begin{cases} v_n + \Delta_n & \text{at} \quad g_n \leqslant G_n \\ v_n + a_n\tau & \text{at} \quad g_n > G_n, \end{cases} \tag{A4}$$

$$\Delta_n = \max\,(-b_n\tau,\ \min(a_n\tau,\ v_{\ell,n} - v_n)), \tag{A5}$$

where $n = 0,1,2,\ldots$ is number of time steps, x_n is the vehicle coordinate at time step n, v_n is the vehicle speed at time step n, a is the maximum acceleration, v_{free} is a maximum speed in free flow, $\tilde{v}_n$ is the vehicle speed without speed fluctuations ξ_n, $v_{s,n}$ is a safe speed at time step n, and v_{free}, a, and d are constants; ℓ marks the preceding vehicle, G_n is a synchronization gap, and a space gap g_n is equal to

$$g_n = x_{\ell,n} - x_n - d. \tag{A6}$$

Functions incorporated in the model can be found in Tables I–VI. Model parameters [58,59] that include "usual" speed adaptation parameters are given in Table VII.

APPENDIX B: PHYSICS OF STOCHASTIC DESCRIPTION OF DIRVER'S SPEED ADAPTATION

To simulate the driver's choice of a space gap within the 2D region of synchronized flow [Fig. 1(a)], we use a stochastic description of driver's speed adaptation within this 2D region made in the model (A1)–(A5) [7,57–59]. For a qualitative explanation of this stochastic description, we do not take into account random fluctuations ξ_n and assume that the space

TABLE III. Functions in model III: Synchronization gap G_n.

$$G_n = G(v_n, v_{\ell,n}),$$
$G(u,w) = \max(0,\ \lfloor k\tau u + a^{-1}\phi_0 u(u-w)\rfloor)$,
k ($k > 1$) and ϕ_0 are constants,
$\lfloor z\rfloor$ denotes the integer part of a real number z.

TABLE IV. Functions in model IV: Safe speed $v_{s,n}$.

$$v_{s,n} = \min\left(v_n^{(\text{safe})}, g_n/\tau + v_\ell^{(a)}\right),$$
$$v_\ell^{(a)} = \max\left(0,\ \min\left(v_{\ell,n}^{(\text{safe})}, v_{\ell,n}, g_{\ell,n}/\tau\right) - a\tau\right),$$
$$v_n^{(\text{safe})} = \lfloor v^{(\text{safe})}(g_n,\ v_{\ell,n})\rfloor$$
is taken as that in Ref. [72], $v^{(\text{safe})}$ is a solution of the Gipps's equation [73]
$$v^{(\text{safe})}\tau_{\text{safe}} + X_d(v^{(\text{safe})}) = g_n + X_d(v_{\ell,n}),$$
where τ_{safe} is a safe time gap,
$$X_d(u) = b\tau^2\left(\alpha\beta + \tfrac{\alpha(\alpha-1)}{2}\right),$$
$\alpha = \lfloor u/b\tau\rfloor$ and $\beta = u/b\tau - \alpha$ are the integer and fractional parts of $u/b\tau$, respectively; b is constant.

TABLE V. Lane changing occurring with probability p_c from the right lane to the left lane ($R \to L$) and from the left lane to the right lane ($L \to R$) and safety conditions for lane changing [57].

Incentive conditions for lane changing:
$R \to L$: $v_n^+ \geqslant v_{\ell,n} + \delta_1$ and $v_n \geqslant v_{\ell,n}$,
$L \to R$: $v_n^+ > v_{\ell,n} + \delta_1$ or $v_n^+ > v_n + \delta_1$.
In conditions $R \to L$ and $L \to R$, the value v_n^+ at $g_n^+ > L_a$ and the value $v_{\ell,n}$ at $g_n > L_a$ are replaced by ∞, where L_a is constant.

Safety conditions for lane changing:
rules ($*$): $g_n^+ > \min(v_n\tau, G_n^+)$, $g_n^- > \min(v_n^-\tau, G_n^-)$, where
$G_n^+ = G(v_n, v_n^+)$, $G_n^- = G(v_n^-, v_n)$,
or
rule ($**$): $x_n^+ - x_n^- - d > g_{\text{target}}^{(\min)}$ with $g_{\text{target}}^{(\min)} = \lfloor \lambda v_n^+ + d\rfloor$,
the vehicle should pass the midpoint point
$$x_n^{(m)} = \lfloor (x_n^+ + x_n^-)/2\rfloor$$
between two neighboring vehicles in the target lane, i.e.,
$$x_{n-1} < x_{n-1}^{(m)} \text{ and } x_n \geqslant x_n^{(m)}$$
or
$$x_{n-1} \geqslant x_{n-1}^{(m)} \text{ and } x_n < x_n^{(m)}.$$

Speed after lane changing:
$$v_n = \hat{v}_n,\ \hat{v}_n = \min(v_n^+,\ v_n + \Delta v^{(1)}),$$
in $\hat{v}_n$ the speed v_n is related to the initial lane before lane changing.

Vehicle coordinate after lane changing:
Vehicle coordinate does not changes under the rules ($*$),
and it changes to $x_n = x_n^{(m)}$ under the rule ($**$).
λ, δ_1, $\Delta v^{(1)}$ are constants; superscripts $+$ and $-$ in variables, parameters,
and functions denote the preceding vehicle and the trailing vehicle in the "target" (neighbouring) lane, respectively;
the target lane is the lane into which the vehicle wants to change.
$G(u,w)$ is given in Table III.

TABLE VI. Models of vehicle merging at on-ramp bottlenecks that occurs when a safety rule $(*)$ *or* a safety rule $(**)$ is satisfied [57].

Safety rule $(*)$:

$$g_n^+ > \min(\hat{v}_n\tau, G(\hat{v}_n, v_n^+)), g_n^- > \min(v_n^-\tau, G(v_n^-, \hat{v}_n)),$$
$$\hat{v}_n = \min\left(v_n^+, v_n + \Delta v_r^{(1)}\right),$$

in $\hat{v}_n$ the speed v_n is related to the initial lane before lane changing, $\Delta v_r^{(1)} > 0$ is constant.

Safety rule $(**)$:

$$x_n^+ - x_n^- - d > \lfloor \lambda_b v_n^+ + d \rfloor,$$
$$x_{n-1} < x_{n-1}^{(m)} \text{ and } x_n \geqslant x_n^{(m)}, \text{ or}$$
$$x_{n-1} \geqslant x_{n-1}^{(m)} \text{ and } x_n < x_n^{(m)},$$

λ_b is constant.

Parameters after vehicle merging:

$$v_n = \hat{v}_n.$$

Under the rule $(*)$: x_n maintains the same,
under the rule $(**)$: $x_n = x_n^{(m)}$.

Speed adaptation before vehicle merging:

$$v_{c,n} = \begin{cases} v_n + \Delta_n^+ & \text{at } g_n^+ \leqslant G(v_n, \hat{v}_n^+), \\ v_n + a_n\tau & \text{at } g_n^+ > G(v_n, \hat{v}_n^+), \end{cases}$$
$$\Delta_n^+ = \max(-b_n\tau, \min(a_n\tau, \hat{v}_n^+ - v_n)),$$
$$\hat{v}_n^+ = \max\left(0, \min\left(v_{\text{free}}, v_n^+ + \Delta v_r^{(2)}\right)\right),$$

$\Delta v_r^{(2)}$ is constant.

TABLE VII. Model parameters [58,59].

Vehicle motion in road lane:
$\tau_{\text{safe}} = \tau = 1, d = 7.5\ \text{m}/\delta x, \delta x = 0.01\ \text{m},$
$v_{\text{free}} = 30\ \text{ms}^{-1}/\delta v, b = 1\ \text{ms}^{-2}/\delta a, \delta v = 0.01\ \text{ms}^{-1},$
$\delta a = 0.01\ \text{ms}^{-2}, k = 3, p_1 = 0.3, \phi_0 = 1, p_b = 0.1,$
$p_a = 0, p^{(0)} = 0.005, p_0(v_n) = 0.575 + 0.125\min(1, v_n/v_{01}),$
$a^{(b)}(v_n) = 0.2a$
$+0.8a\max(0, \min(1,(v_{22} - v_n)/\Delta v_{22}),$
$a^{(0)} = 0.2a, \kappa = 1.8, a^{(a)} = 0,$
$v_{22} = 12.5\ \text{ms}^{-1}/\delta v, \Delta v_{22} = 2.778\ \text{ms}^{-1}/\delta v,$
$v_{01} = 10\ \text{ms}^{-1}/\delta v, v_{21} = 15\ \text{ms}^{-1}/\delta v, a = 0.5\ \text{ms}^{-2}/\delta a.$
"Usual" (weak) speed adaptation parameters are
$p_2(v_n) = 0.48 + 0.32\Theta(v_n - v_{21}), p_1 = 0.3.$

Lane changing:
$\delta_1 = 1\ \text{ms}^{-1}/\delta v, L_a = 150\ \text{m}/\delta x,$
$p_c = 0.2, \lambda = 0.75, \Delta v^{(1)} = 2\ \text{ms}^{-1}/\delta v.$

Bottleneck models:
$\lambda_b = 0.75$ for all the bottlenecks,
$L_c = 1.0\ \text{km}/\delta x$ for off-ramp bottleneck,
$v_{\text{free on}} = 22.2\ \text{ms}^{-1}/\delta v, v_{\text{free off}} = 25\ \text{ms}^{-1}/\delta v,$
$\Delta v_r^{(2)} = 5$ and $-2.5\ \text{ms}^{-1}/\delta v$
for on- and off-ramp bottlenecks, respectively,
$L_r = 1\ \text{km}/\delta x, \Delta v_r^{(1)} = 10\ \text{ms}^{-1}/\delta v,$
$L_m = 0.3$ and $0.5\ \text{km}/\delta x$
for on- and off-ramp bottlenecks, respectively.

gap to the preceding vehicle g_n is within this 2D region of synchronized flow states (Fig. 1) [74]:

$$g_{\text{safe},n} < g_n < G_n, \tag{B1}$$

where the safe space gap $g_{\text{safe},n}$ is found from equation $v_n = v_{s,n}$; that is, under condition (B1) the speed is lower than the safe speed: $v_n < v_{s,n}$. The driver's speed adaptation effect occurs when a driver moves initially with a higher speed than the speed of the preceding vehicle:

$$v_n > v_{\ell,n} > 0, \tag{B2}$$

and the driver cannot overtake the preceding vehicle. In this case the driver should decelerate. This vehicle deceleration adapting the vehicle speed to the speed of the preceding vehicle is described through the use of stochastic deceleration b_n in Eq. (A5). This stochastic deceleration depends on whether the vehicle decelerates at time step n or not (see formula defining b_n in Table II of Appendix A).

If the vehicle does not decelerate at time step n, then the stochastic deceleration b_n in Eq. (A5) is equal to

$$b_n = a\Theta(p_1 - r_1), \tag{B3}$$

where $r_1 = \text{rand}()$, $\Theta(z) = 0$ at $z < 0$, and $\Theta(z) = 1$ at $z \geqslant 0$. In this case, with probability p_1, the vehicle, which did not decelerate at time step n, begins to decelerate at time step $n + 1$ trying to approach the speed of the preceding vehicle. However, from (B3) we also see that with probability $1 - p_1$ the deceleration $b_n = 0$, that is, the vehicle does not begin to decelerate at time step $n + 1$ although in accordance with (B2) the vehicle speed is higher than the speed of the preceding vehicle.

If the vehicle decelerates at time step n, then b_n instead of (B3) in Eq. (A5):

$$b_n = a\Theta(p_2 - r_1). \tag{B4}$$

Thus with probability p_2 the vehicle continues its deceleration at time step $n + 1$ trying to approach the speed of the preceding vehicle; however, with probability $1 - p_2$ the vehicle deceleration $b_n = 0$, that is, the vehicle *interrupts* its deceleration, although in accordance with (B2) the vehicle speed is higher than the speed of the preceding vehicle.

[1] A. D. May, *Traffic Flow Fundamentals* (Prentice-Hall, Englewood, Cliffs, NJ, 1990); M. Cremer, *Der Verkehrsfluss auf Schnellstrassen* (Springer, Berlin, 1979); W. Leutzbach, *Introduction to the Theory of Traffic Flow* (Springer, Berlin, 1988); N. H. Gartner, C. J. Messer, and A. Rathi, editors, *Traffic Flow Theory* (Transportation Research Board, Washington, DC, 2001); D. C. Gazis, *Traffic Theory* (Springer, Berlin, 2002); D. Chowdhury, L. Santen, and A. Schadschneider, Phys. Rep. **329**, 199 (2000); D. Helbing, Rev. Mod. Phys. **73**, 1067 (2001); T. Nagatani, Rep. Prog. Phys. **65**, 1331 (2002); K. Nagel, P. Wagner, and R. Woesler, Operation Res. **51**, 681 (2003); R. Mahnke, J. Kaupužs, and I. Lubashevsky, Phys. Rep. **408**, 1 (2005).

[2] At a given speed, a "timid" driver that exhibits a longer reaction time chooses a greater optimal (safe) gap, whereas an "aggressive" driver that exhibits shorter reaction time chooses a smaller optimal gap than that chosen by an "usual" driver [1].

[3] B. S. Kerner, Phys. Rev. Lett. **81**, 3797 (1998); Trans. Res. Rec. **1678**, 160 (1999); Phys. World **12**(8), 25 (1999).
[4] B. S. Kerner, Phys. Rev. E **65**, 046138 (2002).
[5] B. S. Kerner, *The Physics of Traffic* (Springer, Berlin, 2004).
[6] B. S. Kerner, *Introduction to Modern Traffic Flow Theory and Control* (Springer, New York, 2009).
[7] B. S. Kerner and S. L. Klenov, J. Phys. A: Math. Gen. **35**, L31 (2002).
[8] B. S. Kerner, S. L. Klenov, and D. E. Wolf, J. Phys. A: Math. Gen. **35**, 9971 (2002).
[9] L. C. Davis, Phys. Rev. E **69**, 016108 (2004).
[10] H. K. Lee, R. Barlović, M. Schreckenberg, and D. Kim, Phys. Rev. Lett. **92**, 238702 (2004).
[11] R. Jiang, Q.-S. Wu, J. Phys. A: Math. Gen. **37**, 8197 (2004).
[12] B. S. Kerner and S. L. Klenov, J. Phys. A: Math. Gen. **37**, 1 (2004).
[13] B. S. Kerner and S. L. Klenov, J. Phys. A: Math. Gen. **39**, 1775 (2006).
[14] K. Gao, R. Jiang, S.-X. Hu, B.-H. Wang, and Q.-S. Wu, Phys. Rev. E **76**, 026105 (2007).
[15] L. C. Davis, Physica A **368**, 541 (2006).
[16] L. C. Davis, Physica A **361**, 606 (2006).
[17] L. C. Davis, Physica A **387**, 6395 (2008).
[18] L. C. Davis, Physica A **388**, 4459 (2009).
[19] L. C. Davis, Physica A **389**, 3588 (2010).
[20] L. C. Davis, Physica A **391**, 1679 (2012).
[21] R. Jiang, M.-B. Hua, R. Wang, and Q.-S. Wu, Phys. Lett. A **365**, 6 (2007).
[22] R. Jiang and Q.-S. Wu, Phys. Rev. E **72**, 067103 (2005).
[23] R. Jiang and Q.-S. Wu, Physica A **377**, 633 (2007).
[24] R. Wang, R. Jiang, Q.-S. Wu, and M. Liu, Physica A **378**, 475 (2007).
[25] A. Pottmeier, C. Thiemann, A. Schadschneider, and M. Schreckenberg, in *Traffic and Granular Flow'05*, edited by A. Schadschneider, T. Pöschel, R. Kühne, M. Schreckenberg, and D. E. Wolf (Springer, Berlin, 2007), pp. 503–508.
[26] X. G. Li, Z. Y. Gao, K. P. Li, and X. M. Zhao, Phys. Rev. E **76**, 016110 (2007).
[27] B. S. Kerner, S. L. Klenov, and A. Brakemeier, e-print arXiv:0712.2711v1.
[28] B. S. Kerner, S. L. Klenov, and A. Brakemeier, in *Proceedings of 2008 IEEE Intelligent Vehicles Symposium* (Eindhoven, Netherlands, 2008), pp. 180–185; B. S. Kerner, S. L. Klenov, and A. Brakemeier, in *Proceedings of 4th Int. Workshop V2VCOM 2008* (Eindhoven, Netherlands, 2008), pp. 57–63.
[29] J. J. Wu, H. J. Sun, and Z. Y. Gao, Phys. Rev. E **78**, 036103 (2008).
[30] K. Gao, R. Jiang, B.-H. Wang, and Q.-S. Wu, Physica A **388**, 3233 (2009).
[31] B. Jia, X.-G. Li, T. Chen, R. Jiang, and Z.-Y. Gao, Transportmetrica **7**, 127 (2011).
[32] J-F. Tian, B. Jia, X-G. Li, R. Jiang, X-M. Zhao, and Z-Y. Gao, Physica A **388**, 4827 (2009).
[33] S. He, W. Guan, and L. Song, Physica A **389**, 825 (2009).
[34] Cheng-Jie Jin, Wei Wang, Rui Jiang, and Kun Gao, J. Stat. Mech. (2010) P03018.
[35] B. S. Kerner, S. L. Klenov, and A. Brakemeier, e-print arXiv:0910.0381v2; Traf. Eng. Cont. **51**, 217 (2010); B. S. Kerner, S. L. Klenov, and A. Brakemeier, in *Proceedings of the Transportation Research Board 2010 Annual Meeting* (TRB, Washington, DC, 2010), paper 10-0456.
[36] B. S. Kerner, e-print arXiv:1012.5159v2.
[37] S. Kokubo, J. Tanimoto, and A. Hagishima, Physica A **390**, 561 (2011).
[38] Hyun Keun Lee and Beom Jun Kim, Physica A **390**, 4555 (2011).
[39] Cheng-Jie Jin and Wei Wang, Physica A **390**, 4184 (2011).
[40] J. P. L. Neto, M. L. Lyra, and C. R. da Silva, Physica A **390**, 3558 (2011).
[41] Peng Zhang, Chun-Xiu Wu, and S. C. Wong, Physica A **391**, 456 (2012).
[42] R.-P. Schäfer, S. Lorkowski, N. Witte, J. Palmer, H. Rehborn, and B. S. Kerner, Traf. Eng. Cont. **52**, 225 (2011); B. S. Kerner, H. Rehborn, J. Palmer, and S. L. Klenov, *ibid*. **52**, 141 (2011); J. Palmer, H. Rehborn, and B. S. Kerner. *ibid*. **52**, 183 (2011).
[43] B. S. Kerner. J. Phys. A: Math. Theor. **44**, 092001 (2011).
[44] B. S. Kerner and S. L. Klenov, J. Phys. A: Math. Theor. **43**, 425101 (2010).
[45] B. S. Kerner, S. L. Klenov, and M. Schreckenberg, Phys. Rev. E **84**, 046110 (2011).
[46] B. S. Kerner, Physica A **355**, 565 (2005); IEEE Trans. on Intel. Trans. Sys. **8**, 308 (2007); Traf. Eng. Cont. **48**, 28 (2007); **48**, 68 (2007); **48**, 114 (2007); Trans. Res. Rec. **1999**, 30 (2007); **2088**, 80 (2008).
[47] F. Knorr and M. Schreckenberg, Physica A **391**, 2225 (2012).
[48] S. Lee, B. Heydecker, Y. H. Kim, and E.-Y. Shon, J. Adv. Trans. **4**, 143 (2011).
[49] J.-F. Tian, Z.-Z. Yuana, M. Treiber, B. Jia, and W.-Y. Zhanga, Physica A **391**, 3129 (2012).
[50] The term *hypothetical* state of homogeneous synchronized flow emphasizes that three-phase theory is a qualitative one, which postulates *dynamic features* of hypothetical states of synchronized flow that are assumed to be homogeneous in time and space. Naturally, in a microscopic three-phase traffic flow model, which formulates rules of vehicle motion with the use of the fundamental hypothesis of three-phase theory, small driver fluctuations already incorporated in the model destroy all hypothetical states of homogeneous synchronized flow when dynamic behavior of traffic flow is simulated. However, dynamic features of the hypothetical states of synchronized flow following from the fundamental hypothesis of three-phase theory play the crucial role in this traffic flow dynamics (see Sec. III B).
[51] For example, at a given flow rate in free flow upstream of a bottleneck q_{in} the strength of an on-ramp bottleneck is the greater the greater the on-ramp inflow q_{on}; the strength of an off-ramp bottleneck increases when the percentage of vehicles going to the off ramp increases.
[52] It must be noted that three-phase theory is a qualitative theory in which the fundamental hypothesis about the 2D region of synchronized flow steady states is required for the explanation of the subsequent hypotheses of three-phase theory [3]; this explains the term "fundamental hypothesis." However, as emphasized in Ref. [5] (see pp. 101 and 102), this fundamental hypothesis of *qualitative* three-phase theory should not necessarily be a hypothesis of a *mathematical* three-phase model. In other words, the 2D region of synchronized flow steady states is *not* a requirement for a mathematical three-phase model to exhibit F → S → J transitions and some of the features of congested

patterns [13] (see also Sec. 12.1 of Ref. [6]) as predicted in three-phase theory [3–5].

[53] In this article we try to answer on this question by analyzing results from simulations using a three-phase model that incorporates the fundamental hypothesis of three-phase theory. Naturally, the physics of a *particular mathematical* three-phase model does not exactly equate to the understanding the physics of three-phase theory that is a qualitative one. Therefore, with the approach used in the article we can probably disclose only some of the physical features of the fundamental hypothesis of three-phase theory.

[54] [http://ngsim.camsys.com/].

[55] H. Rehborn, S. L. Klenov, and J. Palmer, Physica A **390**, 4466 (2011).

[56] In the context of three-phase theory, traffic flow of identical drivers and vehicles consists of the same vehicles driven by drivers, which exhibit the same reaction time, the same synchronization gap, and the same safe gap, as well as the same other safety characteristics.

[57] B. S. Kerner and S. L. Klenov, Phys. Rev. E **68**, 036130 (2003).

[58] B. S. Kerner and S. L. Klenov, Phys. Rev. E **80**, 056101 (2009).

[59] B. S. Kerner and S. L. Klenov, J. Phys. A: Theor. Math. **43**, 425101 (2010).

[60] B. S. Kerner, S. L. Klenov, and A. Hiller, J. Phys. A: Math. Gen. **39**, 2001 (2006); Nonlin. Dyn. **49**, 525 (2007).

[61] B. S. Kerner, S. L. Klenov, A. Hiller, and H. Rehborn, Phys. Rev. E **73**, 046107 (2006).

[62] In Ref. [58] we have shown that in real measured single-vehicle data [54] an initial jam growth (jam nucleation) in synchronized flow can be interrupted over time through the driver's lane changing leading to the subsequent jam dissolution.

[63] This is crucially different in comparison with traffic flow models with a fundamental diagram (see Ref. [1] and Sec. 12.1 in Ref. [6]), that is, when there is a single space-gap–speed relationship for a model steady state in congested traffic. This is because there is a direct connection between this space-gap–speed relationship and safety characteristics of a driver in these models [1]: A driver with particular safety characteristics chooses *only one space gap at a given speed* in the model steady state associated with the space-gap–speed relationship. In contrast, in the Kerner-Klenov three-phase model used in this article there is *no* connection between safety characteristics of a driver and the driver's choice of a space gap within the 2D region of synchronized flow states: A driver with *given safety characteristics* chooses *an arbitrary space gap* (arbitrary time headway) at a given speed associated with the 2D region of synchronized flow.

[64] In contrast with traffic flow of identical drivers and vehicles [56], heterogeneous traffic flow consists of drivers with different safety characteristics and/or different vehicles. In particular, a timid driver [2] chooses probably a greater synchronization gap G, a greater safe gap g_{safe} as well as longer driver time delays related to safety driving than an usual driver; an aggressive driver chooses probably a smaller synchronization gap G, a smaller safe gap g_{safe} as well as shorter driver time delays related to safety driving in comparison with the usual driver.

[65] This is crucially different from the KKS cellular automata model [45] in which at a constant value of the probability p in the rule "randomization" the slow-to-start rule is *not* realized, and, therefore, no wide moving jams can propagate in synchronized flow.

[66] Recall [3,5] that synchronized flow states below the line J [labeled by J in Fig. 12(g)], which represents the steadily propagation of the downstream front of a wide moving jam in the flow-density plane, are stable with respect to wide moving jam emergence, whereas synchronized flow states on and above the line J are metastable with respect to this jam emergence. In addition, at the same synchronized flow speed, the closer the space gap to the safe gap associated with the upper boundary of 2D region of synchronized flow, the greater the probability of wide moving jam emergence in synchronized flow during the same time interval of observation.

[67] Following individual vehicles in strong speed adaptation simulations we have found that on average all drivers decelerate more within the 2D region of synchronized flow states than in the case of a weaker speed adaptation. Because in all simulations of strong speed adaptation presented in Secs. II and III we have chosen $p_2 = 1$ in Eqs. (2) and (4), all drivers decelerate to the speed of the preceding vehicle without interruption; in this case the stochastic feature of the strong speed adaptation is associated with probability $p_1 < 1$ of the beginning of this deceleration. When under strong speed adaptation we choose $p_2 < 1$ (Sec. IV A), the probability that a driver decelerates consistently (that is, without interruption in deceleration) is usually small because this is equal to $(p_2)^m$, where $m \geqslant 1$ is the number of time steps required for driver's deceleration to the speed of the preceding vehicle.

[68] Boris S. Kerner, Physica A **333**, 379 (2004).

[69] Because a number of vehicles is always an *integer* value and the flow rate q is defined through the formula

$$q = \frac{\Delta N}{\Delta T},$$

where ΔN is a number of vehicles that have passed a chosen road location during a time interval ΔT, the conclusion about the existence of the *infinite* number of capacities of free flow at the bottleneck within the flow rate range (5) might cause some confusion. To explain this, note that although ΔN is an integer value, ΔT should *not* necessarily be an integer value, that is, ΔT can be a *fractional* value. Therefore, the flow rate q can also be a fractional value; this explains why within the flow rate range (5) there are an *infinite* number of the flow rates, all of which are capacities of free flow at the bottleneck. Indeed, a time interval ΔT in the above-mentioned formula for the flow rate q is determined through formula

$$\Delta T = \sum_{i=1}^{\Delta N} \tau_i^{(\text{gross})},$$

where

$$\tau_i^{(\text{gross})} = t_{i,\text{b}} - t_{i-1,\text{b}}$$

is the gross time headway between two vehicles $i-1$ and i following one after another measured at the road location, $t_{i,\text{b}}$ is a time instant at which the beginning of vehicle i (that is, the vehicle's bumper) reaches this road location. Therefore, the flow rate q can be written as

$$q = \frac{\Delta N}{\Delta T} = \left(\frac{1}{\Delta N} \sum_{i=1}^{\Delta N} \tau_i^{(\text{gross})} \right)^{-1} = \frac{1}{\overline{\tau}^{(\text{gross})}},$$

where $\overline{\tau}^{(\mathrm{gross})}$ is the average gross time headway between vehicles that have passed the road location during the time interval ΔT; obviously, $\overline{\tau}^{(\mathrm{gross})}$ can be an arbitrary value that is larger than zero: $\overline{\tau}^{(\mathrm{gross})} > 0$. Instead of formula $q = 1/\overline{\tau}^{(\mathrm{gross})}$, in traffic engineering an approximation is often used, in which ΔT is considered an *integer* value (a minute, an hour, a day, a month, or else a year). If one forgets the exact formula $q = 1/\overline{\tau}^{(\mathrm{gross})}$, an *incorrect* conclusion might be made that the flow rate should always be an integer value. To illustrate this, let us assume that in the time unit of "minutes" the flow rate measured in accordance with $q = 1/\overline{\tau}^{(\mathrm{gross})}$ is equal to 32.1 vehicles/min. For a person who assumes incorrectly that the flow rate cannot be a fractional value, this result is invalid. However, the same flow rate in the time unit of "hours" is equal to the integer value 1926 vehicles/h; that is, the same flow rate should be considered by the same person as being valid.

[70] An increase in gaps between vehicles is often assumed to be useful for highway traffic control to prevent traffic breakdown or to suppress the emergence of moving jams in synchronized flow (see Chap. 23 in Ref. [5] and Chap. 9 in Ref. [6]). In particular, the increase in space gaps between vehicles can be achieved through the use of vehicle-to-vehicle and/or vehicle-to-infrastructure communication (called V2X communication), which can enhance traffic efficiently and safety as shown in numerical simulations of V2X communnication control integrated into the Kerner-Klenov model [27,28,35] [see, e.g., Figs. 6(c)–6(e) in Ref. [27] as well as Figs. 9.15 and 9.16 in Ref. [6]]. The simulation results of Refs. [27,28,35] have been confirmed in simulations of other microscopic models of synchronized flow [38,47].

[71] To find the probability of S → J transitions, 40 different simulation realizations (runs) during a time interval for observing synchronized flow $T_{\mathrm{ob,SJ}} = 60$ min has been performed. All different realizations (runs) are made at the same flow rates, however, at different initial conditions for model fluctuations in the model [different initial values for functions rand() in Appendix A].

[72] S. Krauß, P. Wagner, and C. Gawron, Phys. Rev. E **55**, 5597 (1997); S. Krauß, Ph.D. thesis, DRL-Forschungsbericht 98-08 (1998) [http://www.zaik.de/paper].

[73] P. G. Gipps, Trans. Res. B **15**, 105 (1981).

[74] Recall [5] that the synchronization gap G and safe gap g_{safe} in Eq. (1) are related to a given vehicle speed under the condition that the speed difference between the preceding vehicle and vehicle $\Delta v_n = v_{\ell,n} - v_n = 0$. In contrast, the synchronization gap G_n and safe gap $g_{\mathrm{safe},n}$ in Eq. (B1) are dynamic variables. For example, when $\Delta v_n > 0$, then at a given speed v_n the value G_n decreases; when $\Delta v_n < 0$, then at a given speed v_n the value $g_{\mathrm{safe},n}$ increases. In each of these cases, the dynamic 2D region of synchronized flow states changes over time. Because G_n and $g_{\mathrm{safe},n}$ are associated with some driver's action points at which driver's behavior changes qualitatively [see associated formulas (A1)–(A5) and formulas in Table IV], the dynamic decrease in G_n and/or increase in $g_{\mathrm{safe},n}$ can lead to a "dynamic jump" from vehicle dynamics associated with dynamic speed adaptation within the dynamic 2D region of synchronized flow to a qualitative another dynamic vehicle behavior. This example may explain a very complex dynamic behavior of vehicles that the model exhibits [57–59].